SYNTHESIS AND CHARACTERIZATION OF NITROGEN DOPED CARBON ELECTROCATALYSTS FOR FUEL CELLS AND AIR BATTERIES ENERGY CONVERSION SYSTEMS

BY

BUKOLA SAHEED ABIDEMI

A Thesis Presented to the

DEANSHIP OF GRADUATE STUDIES

KING FAHD UNIVERSITY OF PETROLEUM & MINERALS

DHAHRAN, SAUDI ARABIA

In Partial Fulfillment of the
Requirements for the Degree of

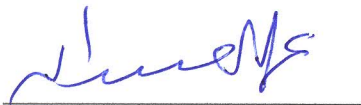# MASTER OF SCIENCE

In

CHEMISTRY DEPARTMENT

DECEMBER, 2013

KING FAHD UNIVERSITY OF PETROLEUM & MINERALS

DHAHRAN- 31261, SAUDI ARABIA

DEANSHIP OF GRADUATE STUDIES

This thesis, written by BUKOLA SAHEED ABIDEMI under the direction his thesis advisor and approved by his thesis committee, has been presented and accepted by the Dean of Graduate Studies, in partial fulfillment of the requirements for the degree of MASTER OF SCIENCE IN CHEMISTRY

Dr. Belabbes Merzougui
(Advisor)

Dr. Al-Hamdan Abdullah Jafar
Department Chairman

Dr. Mazen Khaled
(Member)

Dr. Salam A. Zummo
Dean of Graduate Studies

Dr. Abdel-Nasser Kawde
(Member)

28/12/13

Date

DEDICATION

To the glory of Almighty Allah and to my beloved late father, Sulaiman Iyiola Bukola

ACKNOWLEDGEMENTS

On a final note, I acknowledge the supports of Chemistry department through the Chairman Dr. Al-Hamdan Abdallah Jafar most especially in terms of providing some chemicals used during this research and KFUPM for offering me research assistantship for my MS study.

TABLE OF CONTENTS

LIST OF TABLES

LIST OF FIGURES

LIST OF SCHEMES

LIST OF ABBREVIATIONS

ORR	Oxygen reduction reaction
Pt	Platinum
RDE	Rotating disk electrode
CA	Chronoamperommetry
XPS	X-ray photoelectron spectroscopy
TEM	Transmission electron microscopy
XRD	X-ray diffraction spectroscopy
FESEM	Field emission scanning electron microscopy
EDX	Energy dispersive X-ray spectroscopy
BET	Brunauer–Emmett–Teller
ACB	Acetylene black
PEMFC	Polymer electrolyte membrane fuel cell
DMFC	Direct methanol fuel cell
AFC	Alkaline Fuel cell
SOFC	Solid oxide fuel cell
MCFC	Molten carbonate fuel cell
PAFC	Phosphoric acid fuel cell

ABSTRACT (ENGLISH)

Full Name: Bukola Saheed Abidemi

MS Thesis Title: Synthesis and Characterization of Nitrogen doped Carbon

electrocatalysts for Fuel Cells and Air batteries energy Conversion

systems

Major Field: Chemistry

Date of Degree: December, 2013.

Oxygen evolution and Oxygen reduction reactions (ORR) are critical steps in a variety of energy harvesting and transformation systems (such as fuel cells and air batteries). Currently, Platinum (Pt) based materials are the most convenient cathode catalysts for oxygen reduction reaction (ORR) in fuel cells. But the loss of long term durability as a result of corrosion of the carbon support and Pt dissolution as well as its high cost and limited availability, make Pt-based materials not suitable for the large-scale development of fuel cells and air batteries, in particular. Therefore, the overall objective of the work is to develop potentially efficient platinum-free cathode catalysts to at least circumvent the issue of high cost of Pt and its slow kinetics of the oxygen reduction reaction.

So far as development of Pt-free cathode catalysts are concerned, the major contribution in this work focused on incorporating of a Nitrogen rich source (Polyaniline) on different carbon supports {ketjenblack EC-300 (KB), Vulcan XC-72R (Vulcan), CNT and Acetylene black (ACB)}. The approach is based on polymerization of solid aniline salt on a carbon support using combined Fe^{3+}-/H_2O_2 catalytic system. The synthesis conditions were carefully tailored with the help of the duo oxidants to obtain PANI polymer on carbon

supports which after heat treatment generated highly active sites Fe-N-C for oxygen reduction reaction. Heat treatment is necessary to tune the physicochemical properties of carbon support to form the said Nitrogen doped Carbon electrocatalysts. The obtained catalysts were characterized by using a thin film rotating disk electrode (RDE), Chronoamperommetry test (CA) for its activity towards ORR, methanol tolerance, stability and also by spectroscopy techniques to investigate their morphological structures and composition using XPS (X-ray Photoelectron spectroscopy), TEM (Transmission electron microscopy), XRD (X-ray diffraction technique), Raman spectroscopy, FESEM (High-end Field Emission Scanning electron microscopy), EDX (Energy –dispersive X-ray spectroscopy) and BET area measurement.

ABSTRACT (ARABIC)

الاسم الكامل: سعيد بوكولا ابيدمي

عنوان رسالة الماجستير تركيب وتوصيف لمحفزات النايتروجين الكهربائية المدعم في الكربون لخلايا الوقود والبطاريات الهوائية و أنظمة تحويل الطاقة

حقلالتخصص:الكيمياء

تاريخ الدرجة العلمية: ديسمبر، 2013.

تطور الأكسجين وتفاعل اختزال الأوكسجين هي الخطوات الحاسمة في مجموعة متنوعة من حصاد الطاقة وأنظمة التحويل (مثل خلايا الوقود والبطاريات الهواء).حاليا، المواد البلاتينية هي المحفزات الكاثود الأكثر ملاءمة لتفاعل اختزال الأكسجين في خلايا الوقود. ولكن فقدان قوة التحمل على المدى الطويل نتيجة لتآكل دعامة الكربون وانحلال البلاتينيوم فضلا عن تكلفتها العالية والتوافر المحدود، جعلت مواد البلاتينيوم ليست مناسبة للتطوير على نطاق واسع لخلايا الوقود والبطاريات الجوية، في خاصة. ولذلك، فإن الهدف العام من العمل هو تطوير كفاءة المحفزات المحتملة الكاثود خالية من البلاتين على الأقل الالتفاف على مسألة ارتفاع تكلفة البلاتينيوم وبطء حركة رد الفعل اختزال الأوكسجين.

حتى الآن تطوير المواد الحفازة للقطب السالب الخالية من البلاتينيوم في محل اهتمام، ومساهمة كبيرة في التركيز على إدماج مصدرا غنيا بالنيتروجين)بولي آنلين (على دعامات الكربون المختلفة ويستند هذا النهج على البلمرة لاملاح الأنيلين الصلبة على دعامة الكربون باستخدام نظام تحفيزي مجتمع من Fe^{3+}-/H_2O_2. شروط التركيب كانت مصممة بعناية مع مساعدة من الأكسدة الثنائية للحصول على PANIالبوليمر على دعامات الكربون الذي بعد المعالجة الحرارية ولدت مواقع نشطة للغاية لتفاعل اختزال الأكسجين. المعالجة الحرارية ضرورية لضبط الخصائص الفيزيائية لدعامة الكربون لتشكيل الكربون المرصع بالنيتروجين المحفز الكهربائي وتميزت المحفزات التي تم الحصول عليها باستخدام الطبقة الرقيقة ذات القطب المتناوب RDE، اختبار Chronoamperommetryلنشاطها نحو تفاعل اختزال الأوكسجين والميثانول واستقرارها وأيضا من خلال تقنيات التحليل الطيفي للتحقيق في البنية الشكلية، ومكوناتها باستخدام XPS (الأشعة السينية الضوئية الطيفية) و TEM المجهر الالكتروني

الانتقالي , XRD تقنية حيود الأشعة السينية, FESEM المجهر الالكتروني , EDX الطاقة و تشتت طيق الاشعة, و BET

وقياس المساحة

CHAPTER 1

INTRODUCTION

1.1 General background of Fuel Cells and Batteries

Basically, fuel cell is a device that converts chemical energy into electrical energy. It generates electricity by an electrochemical reaction in which oxygen and a hydrogen-rich fuel combine to form water. In contrary to internal combustion engines, the fuel is not combusted, the energy instead being released electrocatalytically. This allows fuel cells to be highly energy efficient. Fuel cell is similar to a battery in that it generates electricity from an electrochemical reaction. Both convert chemical potential energy into electrical energy and also, as a by-product of this process into heat energy. However, a battery holds a closed store of energy within it and once this is depleted the battery must be discarded, or recharged by using an external supply of electricity to drive the electrochemical reaction in the reverse direction. A fuel cell, on the other hand, uses an external supply of chemical energy and can run indefinitely, as long as it is supplied with a source of hydrogen and a source of oxygen (usually air) [1].

1.2 General Classification of fuel cells

Fuel cells are generally classified according to the nature of the electrolyte used apart from direct methanol fuel cells (DMFC) that use methanol as a fuel.

1.2.1 The Proton Exchange Membrane (PEMFC)

The Proton Exchange Membrane fuel Cell (PEMFC) uses a water-based, acidic polymer membrane as its electrolyte, with platinum-based-electrodes. It operates at very low temperature ($<100^{o}$C) and has capability of tailoring electrical output to meet dynamic power requirements. It is currently the leading technology for light duty vehicles and materials handling vehicles. PEMFC is also sometimes called a Polymer electrolyte membrane fuel cell (PEMFC)

1.2.2 Direct Methanol Fuel Cell (DMFC)

The direct methanol fuel cell (DMFC) is a relatively recent addition to fuel cell technologies. It is similar to the PEMFC in that it uses a polymer membrane as an electrolyte. The catalyst on the anode DMFC (usually platinum-ruthenium) is able to draw the hydrogen from liquid methanol, eliminating the need for a fuel reformer. Methanol offers several advantages as a fuel. It is inexpensive but has a relatively high energy density and can be easily transported and stored. DMFC operates in the temperature range from 60°C to 130°C and tend to be used in applications with modest power requirements, such as mobile electronic devices or chargers and portable power packs.

1.2.3 Solid Oxide Fuel Cell (SOFC)

Solid Oxide fuel cell (SOFC) works at very high temperature around 800°C to 1000°C. SOFCs use a solid ceramic electrolyte, such as Zirconium oxide stabilized with yttrium oxide, instead of liquid or membrane. They are also relatively resistant to small

quantities of sulfur in the fuel, and can hence be used with coal gas. SOFCs find application extensively in large and small stationary power generation.

1.2.4 Alkaline Fuel Cell (AFC)

Alkaline fuel cell (AFC) is one of the first fuel cell technologies to be developed. AFCs use an alkaline electrolyte such as potassium hydroxide (KOH) in water and are generally fuelled with pure hydrogen. Typical operating temperature in modern AFCs is now around 70°C. Nickel is the most commonly used catalyst in AFC units.

1.2.5 Molten Carbonate Fuel Cell (MCFC)

Molten carbonate fuel cell (MCFC) uses a molten carbonate salt suspended in a porous ceramic matrix as the electrolyte. Salts that are commonly used include lithium carbonate, potassium carbonate, and sodium carbonate. It operates at high temperature around 650°C. MFC is used in large stationary power generation.

1.2.6 Phosphoric Acid Fuel Cell (PAFC)

Phosphoric acid fuel cell (PAFC) consists of an anode and a cathode made of a finely dispersed platinum catalyst on carbon and a silicon carbide structure that holds the phosphoric acid electrolyte. They are quite resistant to poisoning by carbon monoxide but tend to have lower efficiency than other fuel cell types in producing electricity. It operates moderately at high temperature of around 180°C. It finds application in stationary power generation and also in large vehicles, such as buses.

Oxygen evolution and reduction reactions are critical steps in a variety of energy harvesting and transformation systems (such as fuel cells, electrolysers and air batteries). Currently, Platinum (Pt) based materials are the most convenient cathode catalysts for

oxygen reduction reaction (ORR), particularly in fuel cells. The problem of slow kinetics of the oxygen reduction reaction (ORR) and high cost associated with platinum based cathode catalyst make the finding of an alternative inexpensive catalyst system indispensable to realize [2,3]. After optimization of the synthesis methods and exploration of various transition-metal and nitrogen precursors, Co$^-$ and Fe$^-$ based catalysts appear as truthfully promising alternatives to platinum [4]. However, there is a debate on the real nature of the active site for the ORR on such non-noble metal catalysts [5]. Yet, it is generally accepted that ORR activity and durability are largely determined by the type of the transition metals in the catalyst, the type of Carbon and Nitrogen precursors used, the ratios of metal/nitrogen,- nitrogen/carbon on the surface, and the synthesis conditions [6].

In this regard, this work focused on incorporating a Nitrogen rich source {Polyaniline (PANI)} on different carbon supports (ketjenblack, Vulcan, CNT and Acetylene black). This was based on the ability of Nitrogen source to complex with Fe precursors ($FeCl_3.6H_2O$) and generate under heat treatment highly active sites able to tune the physicochemical properties of carbon support to form the said Nitrogen doped Carbon Catalysts as electrocatalysts for oxygen reduction reaction. The synthesized catalyst were characterized for its activity, stability, composition and morphology in order to get insight into a deep understanding of the catalytic behavior of Pt-free based catalysts using spectroscopic techniques (XPS, TEM, RAMAN, XRD,SEM and EDX,) and electrochemical techniques {RDE, Chronoamperommetry(CA) and voltamperometry}.

CHAPTER 2

LITERATURE REVIEW

2.1 The development of non-noble metal catalysts

The development of efficient platinum-free catalyst is the key issue to solve the problem of slow kinetics of the oxygen reduction reaction (ORR) and high cost associated with platinum catalysts. Literature survey indicates that non- precious metal (NPM) catalysts based on carbon for oxygen reduction are promising alternatives for platinum based catalysts in fuel cells due to their low cost. However, their activity and durability still do not meet the fuel cell requirements for commercialization.

In 1964, Jasinski first discovered the catalytic nature of cobalt phthalocyanine [7] and later from Gupta's report on transition metal-nitrogen centers as catalytic active sites for ORR [8]. Many approaches have been explored to develop non-noble metal catalysts. Jahnke and Schönborn (1969) applied transition metal phthalocyanine to the non-Pt cathode catalysts in 4.5N H_2SO_4 [9]. Many organometallic complexes have been widely investigated since then. Organometallic complexes have an advantage of easier molecular design as compared to metal-based catalysts. In addition, Jahnke et al (1970s) found that heat treatment of organometallic materials in an inert gas atmosphere enhanced their catalytic activities and stabilities [10]. Furthermore, Yeager and co-workers [11], Van der Putten et al. [12], Van Veen and co-workers [13] and Wiesener [14] have proposed several models to explain the enhancement in activity for ORR.

Alonso-Vante et al. (1986) found that $MO_{4.2}Ru_{1.8}Se_8$ had a superior catalytic activity for the ORR in acidic media [15]. The EXAFS (Extended X-ray Absorption Fine structure) analysis revealed that an O_2 molecule adsorbed on Mo, Ru acted as an active center, and Se affected an electronic state and a local structure of Ru [16].

In 2008, another catalyst family was reported. Akimitsu et al; reported Tantalum (oxy) nitrites (TaOxNy) as new cathode catalyst for polymer electrolyte fuel cells without platinum. TaOxNy films were prepared using a radio frequency magnetron sputtering under $(Ar+ O_2+ N_2)$ atmosphere at substrate temperatures from 50 to 800^oC. The effect of the substrate temperature on the catalytic activity for ORR and properties of TaOxNy films were examined and observed that the catalytic activity of the TaOxNy for the ORR increases with the increasing substrate temperature [17]. Fig 1(a) shows the cyclic Voltammogram (CV) he obtained for the TaOxNy with the substrate temperature of 600^oC and figure 1(b) shows the steady state CVs of the TaOxNy with substrate temperature of 50 and 600^oC. The catalytic activity was investigated for the oxygen reduction reaction in $0.1MH_2SO_4$ at 30^oC with scan rate of $5mVs^{-1}$ as shown in the polarization curve in the figure (2) below.
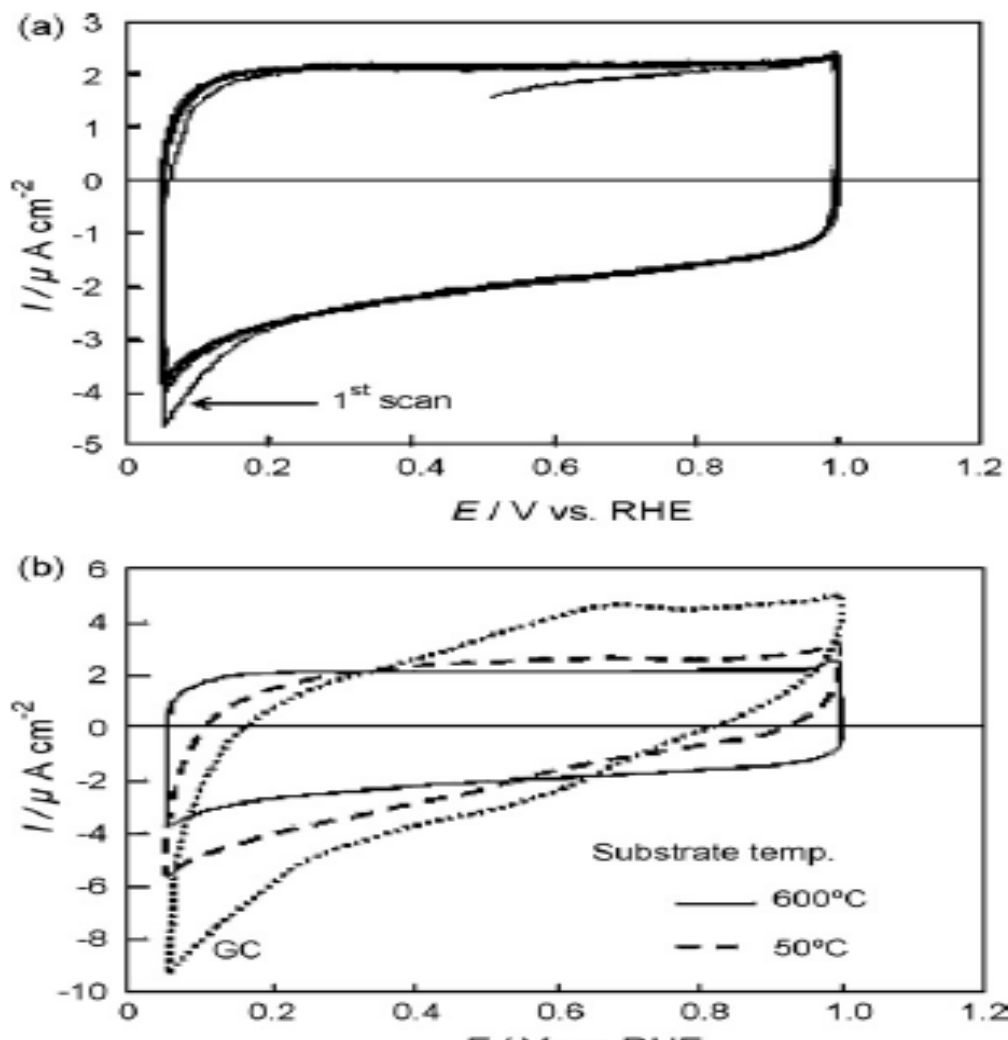
Figure 1(a) Cyclic Voltammogram of the TaOxNy with the substrate temperature of 600°C under N_2 in 0.1 moldm−3 H_2SO_4 at 30°C with a scan rate of 50mVs−1. (b) Steady state cyclic voltamogramm of the TaOxNy under N2 in 0.1moldm−3 H_2SO_4 at 30 °C with a scan rate of 50mVs^{-1}. [Akimitsu, I. et al., Electrochemical Acta 53(2008) 5442-5450]
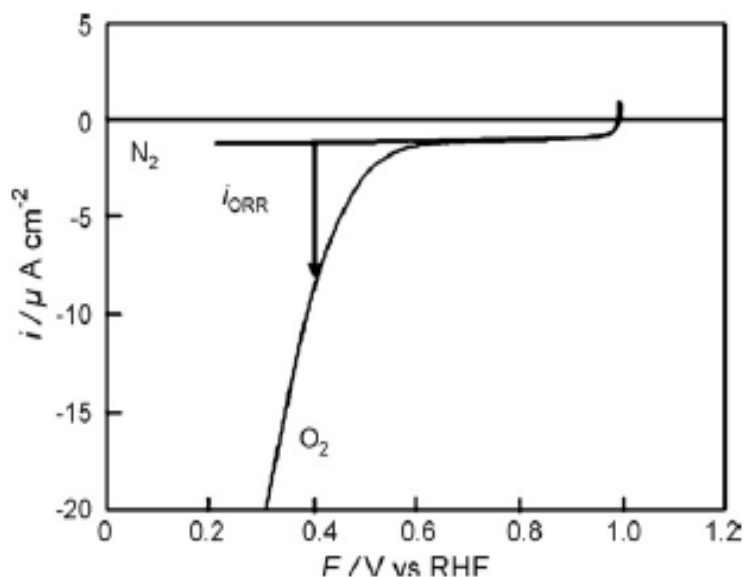
Figure 2: Potential–current curves of the TaOxNy prepared at 800°C under N_2 and O_2 in 0.1 moldm^{-3} H_2SO_4 at 30°C with a scan rate of 5mVs^{-1} .[Akimitsu, I. et al., Electrochemical Acta 53(2008) 5442-5450]

Liangti Q. et al. (2010) developed Nitrogen-doped graphene (N-graphene) by chemical vapor deposition of methane in the presence of ammonia [18]. The resultant N-graphene was demonstrated to act as a metal-free electrode with a much better electrocatalytic activity, long-term operation stability, and tolerance to crossover effect than platinum for oxygen reduction via a four-electron pathway in alkaline fuel cells. In his study, he used a modified Cold Vapor Deposition (CVD) process [19] for the synthesis of N-graphene films. Briefly, a thin layer of nickel (300 nm) was deposited on a SiO$_2$/Si substrate by sputter coating. The Ni-coated SiO$_2$/Si wafer was then heated up to 1000 °C within a quartz tube furnace under a high purity argon atmosphere. Thereafter, a nitrogen-containing reaction gas mixture (NH$_3$:CH$_4$: H$_2$: Ar 10:50:65:200 standard cubic centimeters

8

per minute) was introduced into the quartz tube and kept flowing for 5 min, followed by purging with a flow of NH_3 and Ar only for another 5 min. The sample was then rapidly moved out from the furnace center (1000 °C) under Ar protection. The resultant N-graphene film can be readily etched off from the substrate by dissolving the residual Ni catalyst layer in an aqueous solution of HCl [20], allowing the freestanding N-graphene sheets to be transferred onto substrates suitable for subsequent investigation.

Gang Liu et al. (2010) developed a non-precious nitrogen-modified carbon composite (NMCC) catalyst by the pyrolysis of cobalt, iron–ethylenediamine–chelate complexes on silica followed by chemical and pyrolysis treatments. Pyrolysis temperature and time have a remarkable impact on the content and the type of the nitrogen-containing functional groups in the NMCC catalysts, which affect their catalytic activity and stability. Based on the analysis of the nitrogen functional groups before and after the stability tests, the ORR active sites of the NMCC catalysts are proposed to be pyridinic-N and quaternary-N functional groups. However the pyridinic-N group is not stable in the acidic environment due to the protonation reaction [21, 22].

In 2011, Chi-Web et al. also reported carbon incorporated FeN/C electrocatalysts for oxygen reduction enhancement in direct methanol fuel cells [23]. The C-containing iron nitride electrocatalyst was fabricated by chelating N-containing species and Fe^{2+} with a carbon support under heat treatment in NH_3 atmosphere, which induced the oxygen reduction reaction activity as shown in the figure (3). The electrochemical properties and structures of the catalyst were investigated using X-ray absorption spectroscopy. A rotating disk electrode test was also conducted in sulfuric acid solution and the results revealed the

low H_2O_2 yield and approximately 4e- transfer process of the carbon-containing FeN/C electrocatalyst.
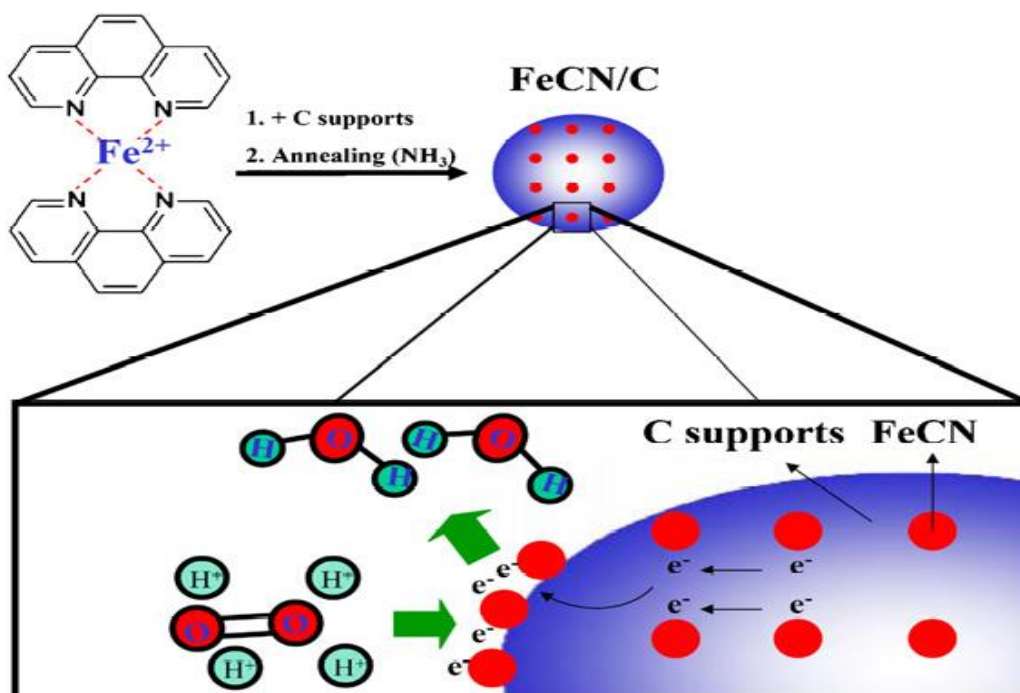
Scheme 1: Schematic representation of FeCN/C electrocatalyst with the formation of Fe_3C and ORR processes. [Chi Wen et al., Electrochimica Acta 56 (2011) 8734-8738

Furthermore, Thangavelu P. (2011) also reported similar non-precious iron nitride-doped carbon nanofibres as cathode catalysts for fuel cells [24]. After realizing the presence of rich defect sites and slit pores along the inner wall of Carbon Nano Fiber (CNF), the morphological feature of CNF was utilized to anchor the FeNx moiety as shown below in figure (4) which led to significant increase in the number of active sites and consequently higher ORR activity.
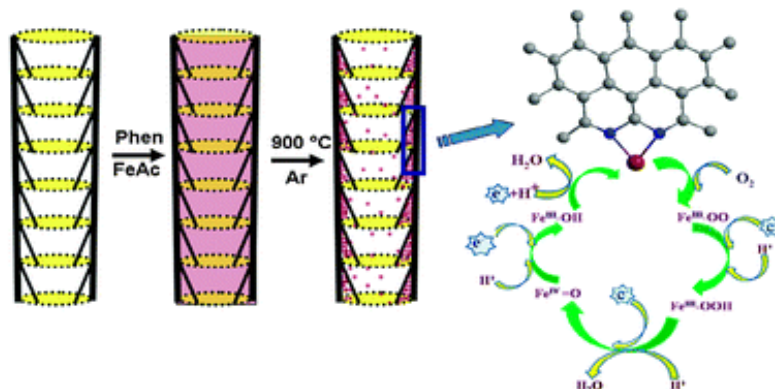
Scheme 2: Proposed pathway of synthesizing FeN$_x$CNF and ORR. N-doped sites are formed along the slit pores and edge sites of the inner wall created due to the cup-stack structure of CNF. [Thangavelu P. et al., Chem. Commun., 2011, 47, 12910-2912]

Similarly, an excellent ORR activity has been reported by Dodelet et al. (2011) by mixing a carbon support with iron precursor, and then heating the materials in ammonia as the source of nitrogen [25, 26]. On the other hand, Zelenay et al. (2011) also achieved high ORR activity by polymerizing the aniline (nitrogen precursor) on high surface area carbon support in the presence of iron precursor and then heating the mixture in an inert gas [27].

Cristina G. et al. (2011) proposed the synthesis of crystalline metal nitride and metal carbide nanostructures by sol-gel chemistry [28]. Generally speaking, in a sol—gel process a solid product or material is formed from a solution, passing by a gel intermediate where both a solid and a liquid phase are present and reactants are mixed at the molecular level. This allows fast reactions and then, lowers working temperatures, and leads to more homogeneous products with higher surface area.

Literature survey shows that comparative study on carbon supports effect on ORR activity with a particular nitrogen precursor in both acidic and alkaline media has not been extensively studied for non-precious metal based catalysts. Polyaniline, polypyrrole and polythiophene have been suggested for applications as active electrode materials in fuel cells, primary and secondary batteries and in super capacitors [29, 30]. Among these polymers, Polyaniline in particular has attracted attention due to its environmental stability, good electrical conductivity and easy synthesis, and also served as efficient matrix for the immobilization of the ORR catalysts on a carbon support as a result of its increased electrochemical surface area and nitrogen rich source [31].

Many investigators have employed ammonium peroxydisulfate {$(NH4)_2S_2O_8$, APS} for the stoichiometric polymerization of aniline on a carbon support as a potential fuel cell electrocatalyst. G. Wu et al. (2011) used APS for polymerization of liquid aniline with ketjenblack carbon (KB) and obtained good ORR activity [32]. Also, Lei Fu et al. (2010) developed activated carbon/PANI with high ORR activity by using the same APS as main oxidant for polymerization of liquid aniline [33]. Furthermore, APS oxidant was also employed by B. Merzougui et al. (2013) to deposit PANI from liquid aniline on multiwalled carbon nanotubes [34]. In an effort to avoid the use of APS as oxidant, Zelenay et al. (2010) of Los Alamos Laboratory came up with a simple synthesis method of sulfur-free approach by employing $FeCl_3$ as the only oxidant for polymerizing liquid aniline to obtain a cathode catalyst [35]. APS is known to be a good oxidant, but its reaction products are sometimes difficult to remove. It has been noticed that formation of sulfur containing compounds, such as FeS which are known to be poison towards oxygen reduction reaction could occur. Using

APS requires several washing of catalyst and sometimes acid treatment, which in most cases require a second heat treatment (a time consuming step).

Therefore, to develop a stable and highly active non-precious catalyst for ORR, it is very important to tailor synthesis method in order to achieve a catalyst with high graphitic nitrogen content [36]. This work focused on development of non-precious metal catalysts using a novel synthesis approach to obtain high yield of Polyaniline on a carbon support by employing solid aniline salt and Fe^{3+}-/H_2O_2 catalytic system.

2.2 Problem Statement

Fuel cells and Air batteries are efficient power generation sources with high efficiency and low emission and will make a significant contribution to the environment protection and the utilization of clean energy in the near future. In a Fuel cell, the oxygen reduction reaction (ORR) rate is slower by six–fold than the oxidation reaction rate of the anode. This makes ORR one of the critical factors limiting the performance of fuel cells. To date, platinum-based materials are the most widely used as electrocatalysts for ORR. However, the problems of durability, scarcity, and high cost of Pt significantly hamper the commercial applications of fuel cells. Since synthesis method has been identified as a determining factor to develop non-precious metal (NPM) catalysts with desirable properties which are known to be Pt-based materials shortcomings. During this work, efforts were made to avoid the problems of some common synthesis approaches. We used solid aniline hydrochloride salt as a monomer for the first time for this application which does not require additional additives owing to its high solubility in water. This is preferred to liquid aniline from the point of view of toxic hazards. To lessen the presence of residual aniline and to obtain the best yield of Polyaniline, we used stoichiometric molar ratio 0.2/0.02/0.4 for

13

aniline/Fe^{3+}/H_2O_2 respectively. To prevent aggregation of PANI precipitate that could reduce the active sites for ORR during heat treatment and to obtain a porous fine powder, ammonium carbonate was used as a sacrificial material to yield voids during heat treatment step. Since oxidative polymerization of aniline is exothermic, temperature influence is an important factor to control as a result the reaction was carried out at 8^0C.

2.3 Research Objectives

1) To obtain a high surface area of modified carbon.

2) To increase active site (increase Nitrogen to Carbon ratio) for ORR activity.

3) To obtain a Fe-N-C composite system that is chemically and electrochemically stable.

4) To obtain a catalyst free of platinum for oxygen reduction reaction in fuel cells development.

5) To characterize the synthesized catalyst using RAMAN, XRD, SEM-EDX, XPS and TEM to provide information about morphology and elemental analysis in order to highlight the active sites towards the oxygen reduction reaction.

6) To evaluate the performance of the catalyst in either acidic or alkaline medium by voltamperometry, rotating disk electrode (RDE), Chronoamperommetry (CA) and half-cell measurements.

7) To investigate the extent of the effect of surface area of carbon supports in ORR activity.

8) To determine the number of electrons transfer so as to propose the Oxygen reduction mechanism for the synthesized catalysts using Koutechy-Levich principle.

CHAPTER 3

RESEARCH METHODOLOGY

3.1 MATERIALS: Vulcan XC-72 purchased from Cabot, USA; ketjenblack EC-300 was obtained from AKZO Nobel, USA; Aniline hydrochloride solid purchased from Eastman Kodac, USA; Multiwall carbon nanotubes (CNTs) purchased from Cheap Tubes Incorporation, USA (http://www.cheaptubesinc.com/) and Acetylene black (ACB) was obtained from JACAAL , USA. MilliQ UV-plus water (Millipore) was used throughout all experiments.

3.2 CATALYSTS SYNTHESIS

3.2.1 First Synthesis trial with $(NH_4)_2S_2O_8$ (APS) oxidant

5.0g of aniline was mixed with 50 ml water. Thereafter, 37% HCl was added dropwise with continuous stirring until aniline became completely miscible with water. Then, 1.0 g of Vulcan carbon was added into the mixture aniline/water and sonicated for 2h in a sonication bath to obtain well dispersed slurry and kept overnight under stirring to impregnate aniline into Vulcan. As an oxidant agent, 10.0 g of ammonium per sulfate $\{(NH_4)_2S_2O_8\}$ was dissolved in water and added in dropwise to the mixture and kept overnight under stirring to ensure proper and complete polymerization. The obtained product, named as PANI/Vulcan was then filtrated and washed with Di-water for several times until pH became less acidic (pH= 6), then dried under vacuum at 80oC overnight. In the next step, 1.0 g of the sample PANI/Vulcan was dispersed in water in form of slurry using ultra sonication. On the other hand, 0.48 g FeCl3.6H2O (to give 10% Fe per wt.) was

dissolved in water and added to the slurry. The mixture was then kept on a magnetic stirrer overnight to ensure complexation of $FeCl_3$ onto PANI/Vulcan. The mixture was vacuum dried at 80^oC and then heat treated in N_2 at 900^oC for 3 hr. The activity measurements indicate a low activity from the synthesized catalyst. This necessitated a second synthesis trial.

3.2.2 Second Synthesis trial with Fe^{3+}-/H_2O_2 catalytic system

The synthesis method involved the initial pretreatment of carbons supports (Vulcan XC-72 and ketjenblack EC300, CNT and Acetylene black) in 40 ml 0.5M HCl overnight, approximately 15 hr. This is necessary to remove any foreign impurities in the carbon supports. The carbon supports were filtered washed with H_2O and vacuum dried at 70^oC for 7 hr. The reaction volume was set at 100ml in order to maintain 0.2/0.02/0.4 molar ratio of aniline salt/Fe^{3+}/H_2O_2 respectively. 0.26 g of the carbon source were dispersed in 40 ml H_2O and sonicated for 20 mins. This was transferred to a water bath maintained at 8^oC using circulating bath. 0.2M aniline hydrochloride salt (2.592 g, 0.02 mol) was dissolved in 40ml H_2O then added to the carbon support. The mixture was kept under stirring for proper impregnation of aniline salt onto carbon matrix. Thereafter, 0.02M $FeCl_3.6H_2O$ (0.512 g, ≈0.002 mol) was dissolved in 10ml water and added to the slurry. 0.4M H_2O_2 (2.68 ml) prepared from 35% H_2O_2 was added in dropwise to the mixture and then make up to 100ml. The mixture was left under stirring for 24 hr to ensure complete polymerization of aniline. The mixture was filtered, washed and seeded with ammonium carbonate (to prevent aggregation of PANI and to create porosity (later after heat treatment)) and thereafter vacuum dried at 80^oC for 7 hr. The same synthesis conditions were repeated for each carbon support. The Scheme 3 below illustrates the proposed synthesis pathway used in this study

and Scheme 4 is the mechanism involved in the oxidative polymerization of aniline salt on a carbon support using Fe^{3+}-/H_2O_2 catalytic system (first part of scheme 3) in which both Fe^{3+} and H_2O_2 were actively involved in the polymerization with only water as by-product. This will believe assisted to have complete polymerization.
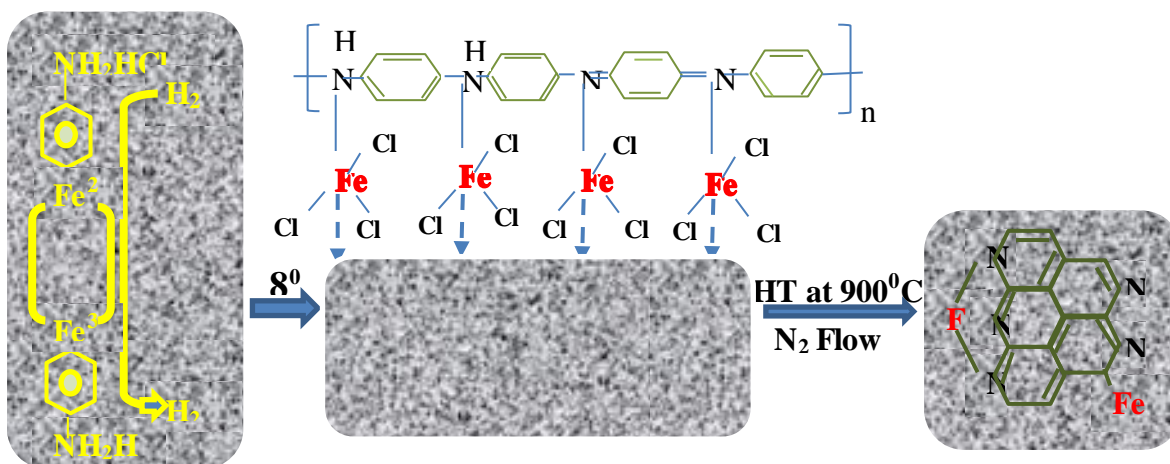
Scheme 3: Proposed synthesis pathway for Fe-N-C catalysts.
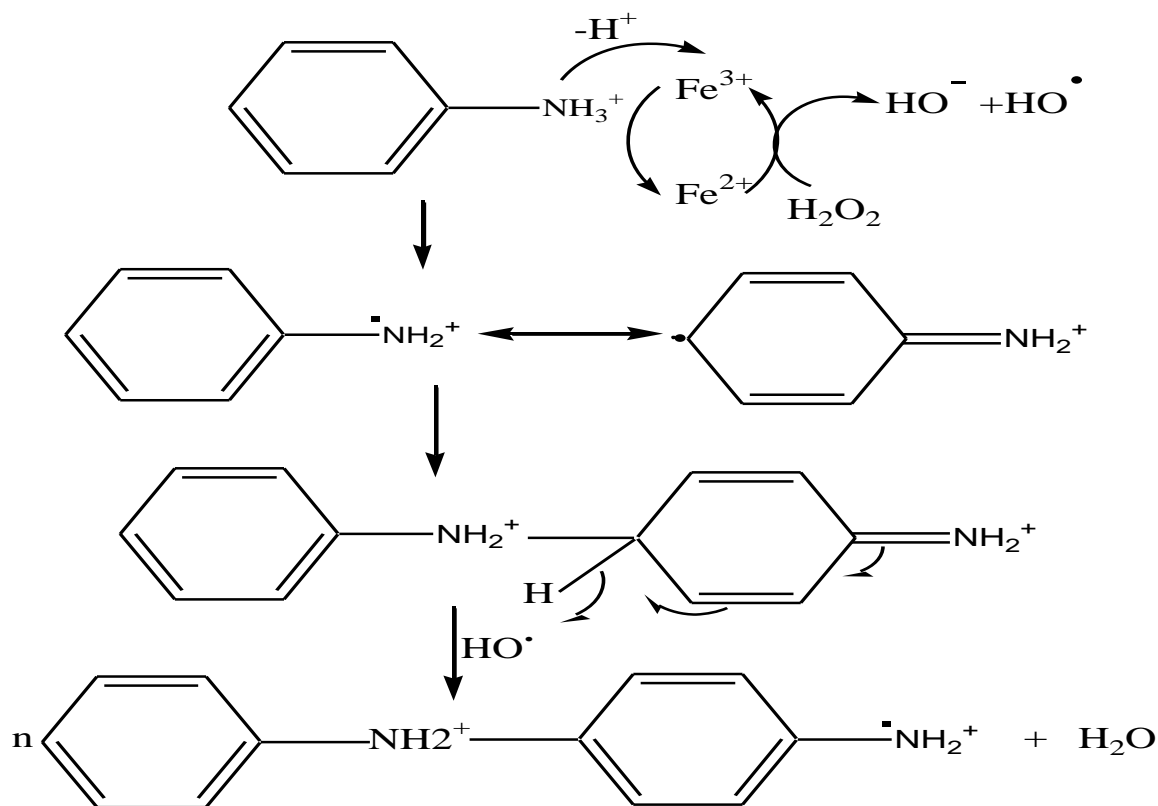
Scheme 4: Proposed catalytic Oxidative polymerization of aniline mechanism using Fe^{3+}-/H_2O_2 catalytic system.

3.3 HEAT TREATMENT

The mixtures obtained from the above step were subjected to heat treatment in 10% N_2 at 900^oC for 1 hr (3 hr for ramping temperature from 25^oC to 900^oC) to obtain nitrogen doped carbon composites with increased active sites for the oxygen reduction reaction (ORR) activity. This is a very crucial step in the synthesis of the said catalyst. Here, the heat treatment could cause structural changes to the carbon supports. These defects could be the host for the formation of pyrrolic, pyridinic and graphitic nitrogen functions, which are believed to be the active sites for oxygen reduction reaction. Heat treatment may also cause creation of pores due to degasification, such as evolution of Cl_2, CO_2, CO and HCl.

Degasification might sometimes be responsible for the increase in real BET area of the catalyst. The MTI furnace used for this purposed is represented in the figure 3 below.

Figure 3:   High temperature Vacuum tube furnace used for the heat treatment of the synthesized catalysts.

Four catalysts were synthesized in this work and were denoted as follows:

(a) Fe-N-C/Ketjenblack

(b) Fe-N-C/Vulcan

(c) Fe-N-C/CNT

(d) Fe-N-C/ACB

CHAPTER 4

RESULTS AND DISCUSSION

4.1 Spectroscopy Characterization

In order to highlight the active sites so as to get insight into a deep understanding of the catalytic behaviors of the synthesized catalysts towards oxygen reduction reaction, spectroscopy characterization were conducted to provide details information about their morphological structures and elemental composition.

4.1.1 RAMAN Spectroscopy

Raman spectra were taken on an iH320 Horiba spectrometer with charge-coupled device (CCD) using monochromatic laser (300mW, 532nm), grating of 1200cm^{-1} and an aluminum substrate. Raman spectroscopy provides information needed to elucidate the morphological changes done to the catalyst by the heat treatment. The intensity ratio of D-band to the G-band obtained from the spectra interprets the degree of disorder occurred in the structure of the carbon supports. The so-called G-line is a characteristic feature of the graphitic layers and corresponds to the tangential vibration of Carbon atoms. The D-line mode is a typical sign for defective graphitic structure [37]. The comparison of the ratios of these two peaks intensities gives a measure of the quality of the catalytic structure. This spectroscopic technique was performed on the synthesized catalysts before and after the heat treatment. The peaks centered at 1334 cm^{-1} and 1595

cm^{-1} are designated as D-band and G-band respectively [38]. The D/G ratios of the four raw carbon and their corresponding catalysts are given in the table 1 below

Raw Carbon	D/G Ratio	Catalysts	D/G Ratio
Ketjenblack	0.39	Fe-N-C/Ketjenblack	0.41
Vulcan XC-72	0.53	Fe-N-C/Vulcan	0.55
CNT	0.21	Fe-N-C/CNT	0.22
Acetylene black	0.297	Fe-N-C/ACB	0.281

Table 1: The D/G ratios of the raw carbon and catalysts obtained from the RAMAN spectra.

The structural changes of the four catalysts as elucidated by Raman spectroscopy are given in the figure 4(a, b, c and d) below. The spectroscopic data (D/G ratios) obtained from Raman spectra of the raw carbon and the synthesized catalysts as also shown in the above table indicate that there were no much structural defects created into the carbon network establishing that the synthesized catalysts are more in their respective graphitic forms.
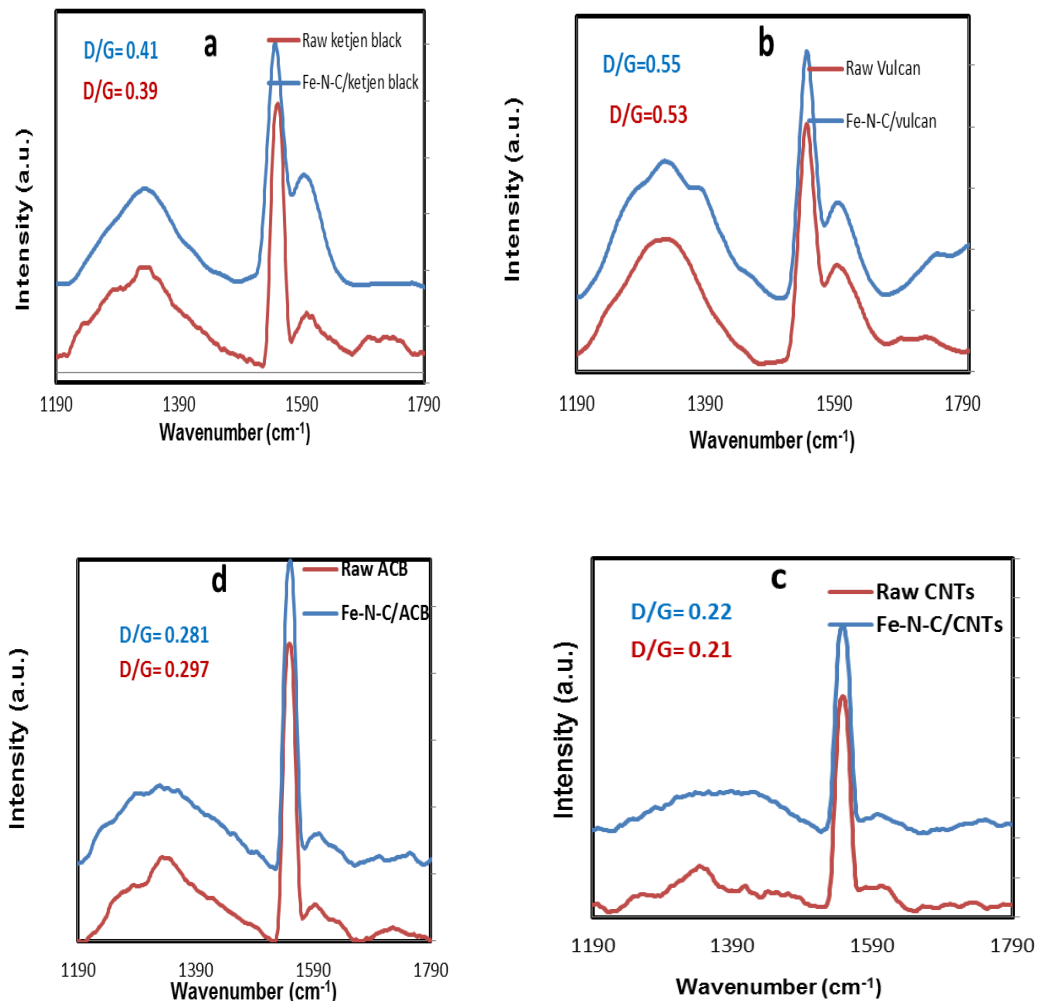
Figure 4: Raman spectra of raw carbon (red) and Fe-N-C (blue) of the synthesized catalysts (a) Fe-N-C/ketjenblack (b) Fe-N-C/Vulcan (c) Fe-N-C/CNT and (d) Fe-N-C/ACBs

4.1.2 X-RAY DIFFRACTION (XRD)

X-ray diffractions (XRD) patterns were collected using a Rigaku Miniflex II instrument with a monochromator of CuKα1 (1.5406Å) at 30kV, 15mA. The XRD patterns were recorded in the static scanning mode from 5° to 60° (2Θ) at a detector angular speed of $2^{o}\Theta min^{-1}$ and step size of 0.02^{o}. XRD is used to obtain the arrangement of particles in a

23

solid. The wavelength of X-rays is approximately the same as distance between the particles in the lattice. If the beam of X-rays strikes a crystal, the X-rays are deflected by the crystal and are detected by a photographic plate. This technique was used to examine the morphological structure of the synthesized catalysts. The four catalysts synthesized during this work show broad diffraction peaks at $25-26^0$ which have been attributed to the (002) carbon in graphitic form. The retention of these strong intensities of the peaks after heat treatment at 900^oC further establish formation of nitrogen-doped carbon without necessarily sacrificing the graphitic form which is in agreement with Raman data. Moreover, the diffraction peaks centred at $43-45^0$ in the two catalysts can be attributed to Fe-N functionalities and Fe nanoparticles. The formation of Fe-N moieties is supported by XPS results which will be discussed shortly. The figure 5 below shows the diffraction patterns of the four catalysts.
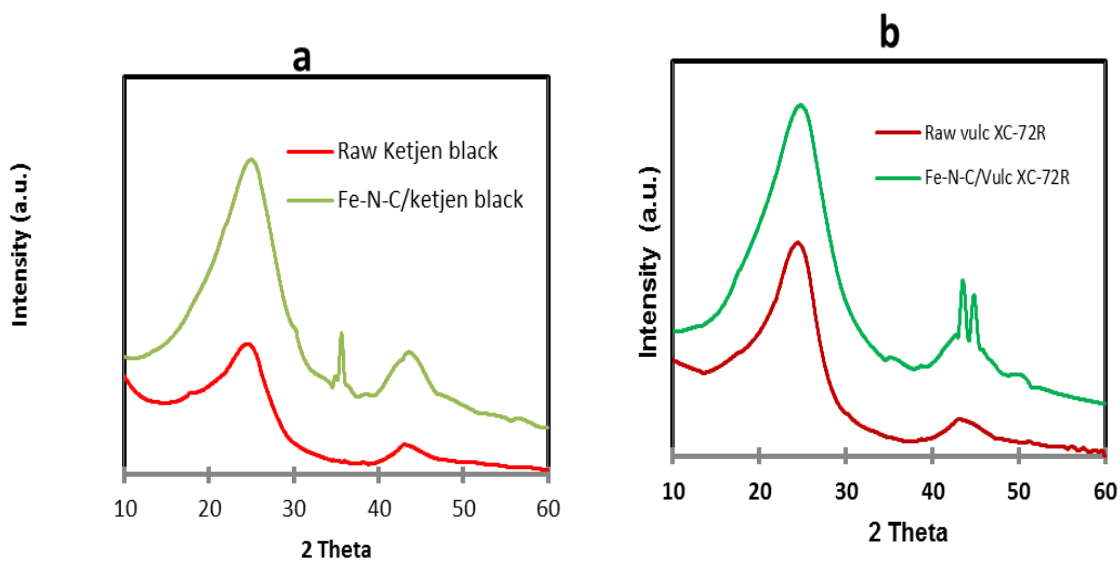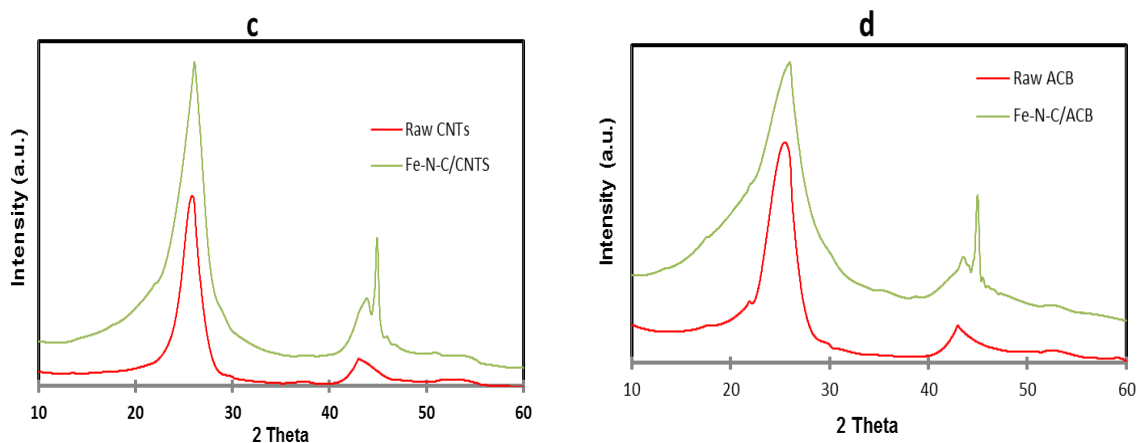
Figure 5: XRD patterns of the synthesized catalysts (a) Fe-N-C/KB (b) Fe-N-C/Vulcan (c) Fe-N-C/CNT and (d) Fe-N-C/ACB

4.1.3 SEM IMAGES

High-end–field emission scanning electron microscope (FESEM, Tescan-Lyra-3) was used to provide images of the synthesized catalysts. Scanning electron microscope (SEM) uses a focused beam of high-energy electrons to generate a variety of signal at the surface of solid specimens. The signals that derive form electron – sample interactions reveal information about the sample including external morphology (texture), chemical composition, and crystalline structure and orientation of materials making up the sample. Accelerated electrons in a SEM carry significant amounts of kinetic energy, and this energy is dissipated as a variety of signals produced by electron – sample interaction when the incident electrons are decelerated in the solid samples. These signals include **secondary electrons** (that produce SEM images), **backscattered electrons** (BSE), **diffracted backscattered electrons** (EBSD) that are used to determine crystal structures and orientations. Secondary electrons are most valuable for showing morphology and topography on samples and

25

backscattered electrons are most valuable for illustrating contrasts in composition in multiphase sample (i.e. for rapid phase discrimination). Figure 6 shows the SEM images of the synthesized catalysts with the same magnification of 2 μm scale bar. The images clearly reveal porous structure as a result of seeding strategy by using ammonium bicarbonate. Porous catalysts have been well reported in the literature and demonstrated high ORR activity than dense catalysts.
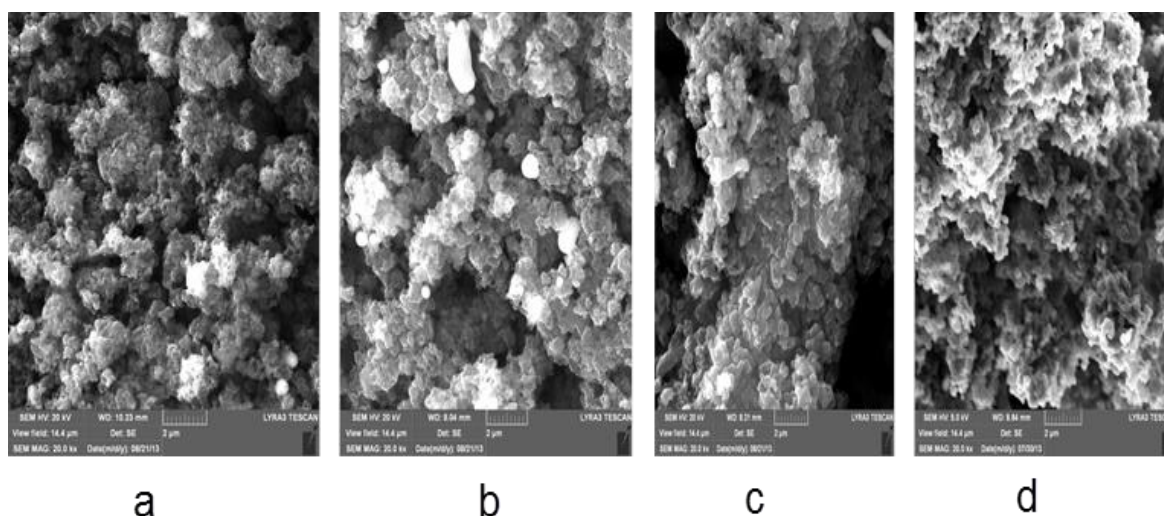
Figure 6: SEM images of the as-synthesized catalysts (a) Fe-N-C/KB (b) Fe-N-C/Vulcan (c) FE-N-C/CNT and (d) Fe-N-C/ACB

4.1.4 EDX spectroscopy

Energy – dispersive X-ray spectroscopy (EDX, Oxford-Xmax) was used to provide preliminary elemental composition information. The identified elements in all the catalysts were in good agreement with other spectroscopic data (XRD and XPS). Table 2 below shows the percentage composition by weight of the identified elements in the synthesized catalysts.

a

Spectrum	In stats.	C	N	O	Fe	Total
Spectrum 1	Yes	84.50	10.06	5.04	0.40	100.00
Spectrum 2	Yes	86.74	8.27	4.41	0.58	100.00
Spectrum 3	Yes	88.05	7.45	4.19	0.31	100.00
Spectrum 4	Yes	89.62	7.60	2.35	0.43	100.00
Spectrum 5	Yes	84.48	11.12	4.00	0.40	100.00
Spectrum 6	Yes	88.28	7.32	4.05	0.35	100.00
Spectrum 7	Yes	84.26	10.03	5.37	0.35	100.00
Mean		86.56	8.84	4.20	0.40	100.00
Std. deviation		2.18	1.54	0.97	0.09	
Max.		89.62	11.12	5.37	0.58	
Min.		84.26	7.32	2.35	0.31	
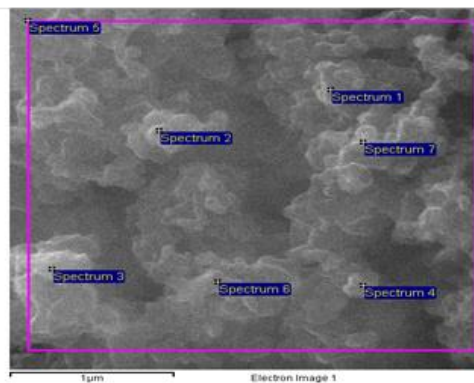
All results in weight%

b

Spectrum	In stats.	C	N	O	Fe	Total
Spectrum 1	Yes	82.98	9.65	2.67	4.70	100.00
Spectrum 2	Yes	75.63	17.24	5.73	1.40	100.00
Spectrum 3	Yes	77.09	17.02	4.26	1.63	100.00
Spectrum 4	Yes	85.98	7.44	3.26	3.32	100.00
Spectrum 5	Yes	76.16	7.41	5.09	11.35	100.00
Spectrum 6	Yes	66.88	12.35	3.07	17.70	100.00
Spectrum 7	Yes	67.38	2.82	1.89	27.92	100.00
Spectrum 8	Yes	64.08	6.20	2.28	27.44	100.00
Spectrum 9	Yes	62.84	1.03	1.94	34.19	100.00
Spectrum 10	Yes	88.07	3.85	1.99	6.09	100.00
Spectrum 11	Yes	78.76	12.22	1.82	7.20	100.00
Mean		75.08	8.84	3.09	12.99	100.00
Std. deviation		8.75	5.43	1.37	11.89	

27
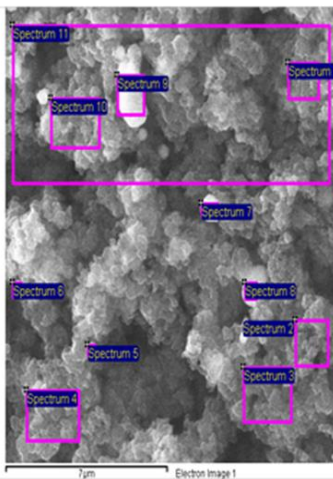
c
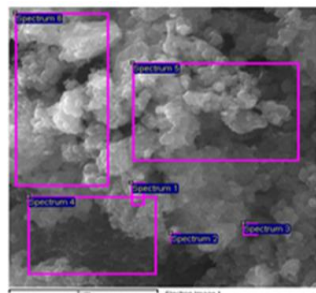
Spectrum	In stats.	C	N	O	Fe	Ni	Total
Spectrum 1	Yes	82.14	6.72	2.22	8.75	0.17	100.00
Spectrum 2	Yes	87.22	6.47	1.18	4.88	0.24	100.00
Spectrum 3	Yes	74.30	8.35	2.91	13.88	0.56	100.00
Spectrum 4	Yes	87.37	7.59	2.43	2.39	0.23	100.00
Spectrum 5	Yes	80.86	12.15	4.53	2.18	0.29	100.00
Spectrum 6	Yes	85.13	9.87	3.81	1.09	0.10	100.00
Mean		82.84	8.52	2.85	5.53	0.27	100.00
Std. deviation		4.95	2.16	1.19	4.93	0.16	
Max.		87.37	12.15	4.53	13.88	0.56	

d
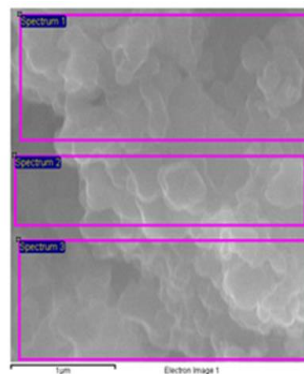
Spectrum	In stats.	C	N	O	Si	Fe	Total
Spectrum 1	Yes	81.64	10.08	7.48	0.21	0.59	100.00
Spectrum 2	Yes	82.16	9.94	7.09	0.24	0.58	100.00
Spectrum 3	Yes	84.41	8.19	6.37	0.27	0.76	100.00
Mean		82.74	9.40	6.98	0.24	0.64	100.00
Std. deviation		1.47	1.05	0.56	0.03	0.10	
Max.		84.41	10.08	7.48	0.27	0.76	
Min.		81.64	8.19	6.37	0.21	0.58	

Table 2. EDX table showing the percentage composition of the catalyst (a) Fe-N-C/KB (b) Fe-N-C/Vulcan (c) Fe-N-C/CNT and (d) Fe-N-C/ACB

Based on the percentage composition illustrated in the above figures, the summary of the average value of each element in each catalyst sample and the ratio of nitrogen/carbon is given in the table 3 below.

Catalysts	C	N	O	Fe	Ni	Si	N/C
Fe-N-C/ketjen black	86.56	8.84	4.20	0.40	---	---	0.10
Fe-N-C/Vulc XC-72R	75.08	8.84	3.09	12.99	---	---	0.12
Fe-N-C/CNTS	82.84	8.52	2.85	5.53	0.27	---	0.10
Fe-N-C/ACB	82.74	9.40	6.98	0.64	---	0.24	0.11

Table 3.   Summary of the average percent by weight of the elements in each catalyst synthesized.

4.1.5 Transmission Electron Microscopy (TEM)

TEM Titan super twin (FEI Co) was used to obtain high resolution transmission electron microscopy (HRTEM) images at 300kV. The TEM images of the best catalysts, Fe-N-C/Ketjenblack and Fe-N-C/Vulcan were taken to have deep understanding of the composition and morphology of the catalyst structure. Fig. 7 and 8 shows TEM images of Fe-N-C/KB and Fe-N-C/Vulcan catalysts respectively, where a thin layer of Fe nanoparticles are embedded in the graphitic structure of the carbon.
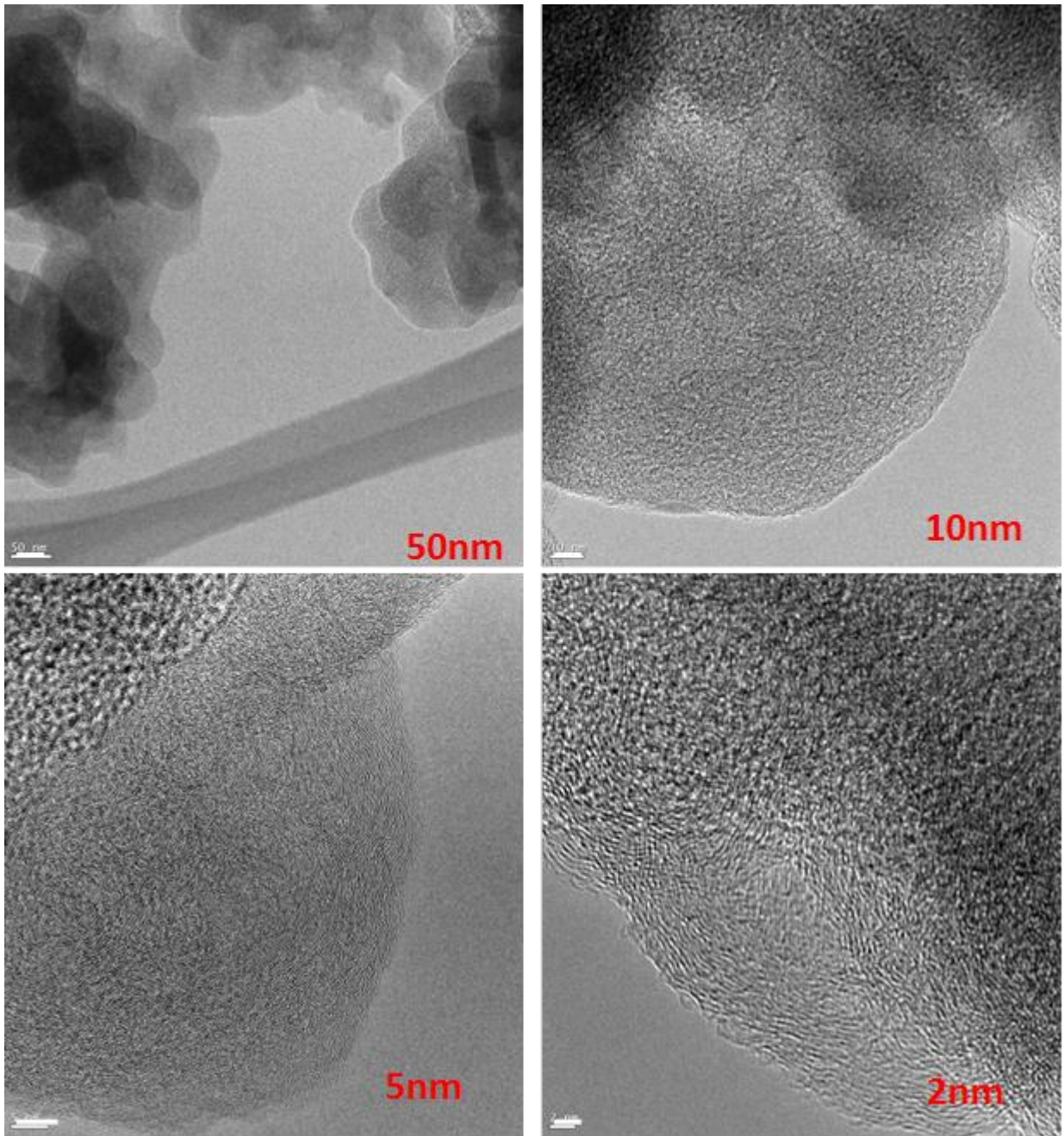
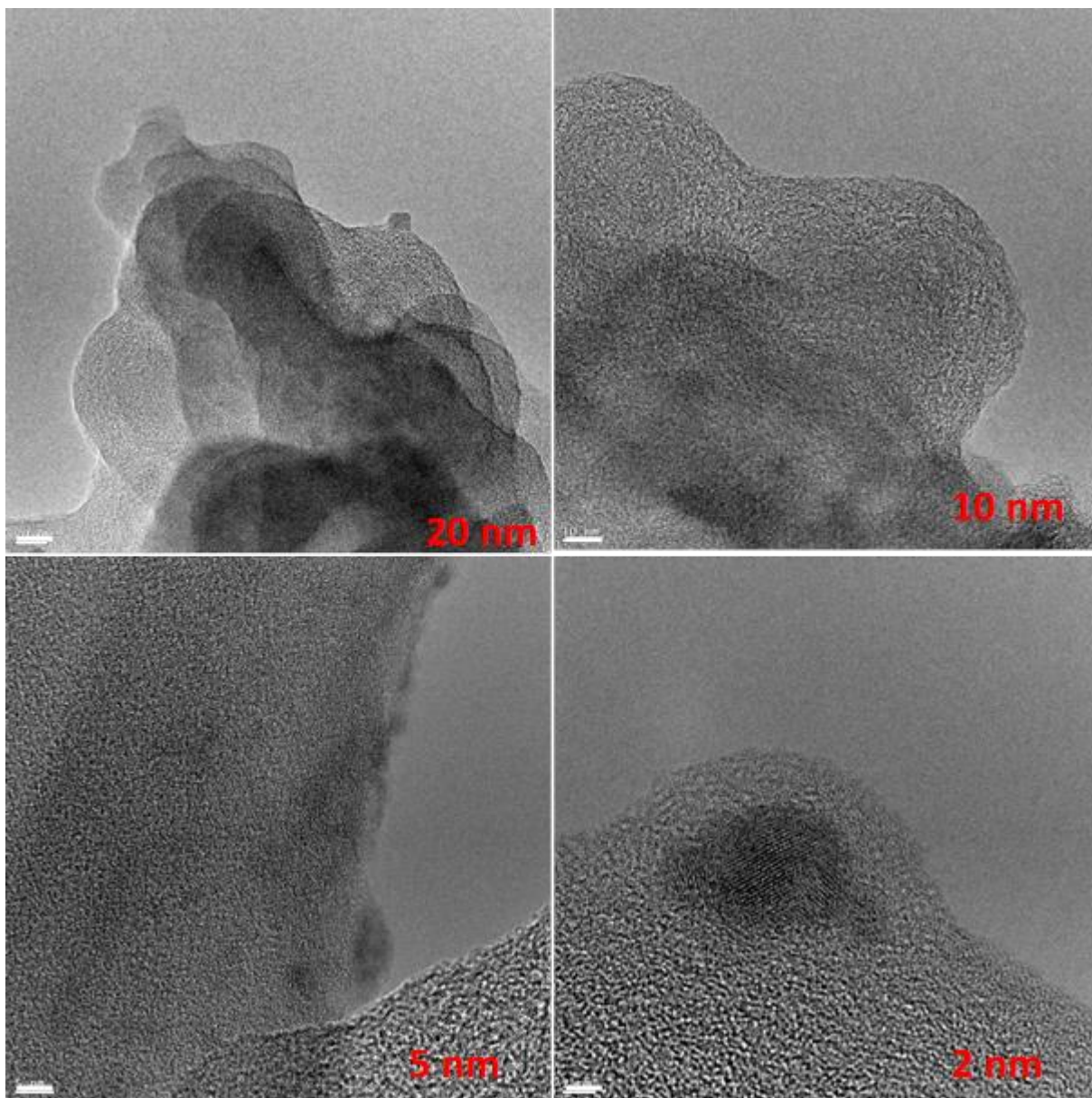Figure 7: TEM images of Fe-N-C/ketjenblack

Figure 8: TEM images of Fe-N-C/Vulcan

4.1.6 X-ray Photoelectron Spectroscopy (XPS)

Furthermore, XPS spectra for the best two catalysts were analysed to elucidate the type of nitrogen groups. The figure 9 and 10 show the spectra of N 1S for Fe-N-C/ketjenblack and Fe-N-C/Vulcan catalysts which comprises of three main peaks centred at 398.1, 400.9, and 405.8 eV, and they are attributed to N-pyridinic, , N-graphitic and N-oxides respectively [39,40]. Furthermore, the deconvoluted spectra fig 11 and 12 show additional shoulder peaks at 399.4 eV and 402 eV attributed to N-"Fe" and N-"O" respectively . Based on the deconvolution of spectra, we estimated the total atomic percentage of Nitrogen to be 2.5 for Fe-N-C/ketjenblack and 3.2 for Fe-N-C/Vulcan, among which N-graphitic represents approximately 42%, N-pyridinic, 17%, and N-"Fe", 10%. It is clear from XPS results that this approach led to catalyst rich in nitrogen graphitic form that is believed to enhance ORR activity and stability [41]. Though, pyridinic-N also promotes high ORR activity but could be prone to protonation especially in acidic medium. . As expected, formation of N-"Fe" moieties may not be ruled out as XPS did in fact reveal the formation of such nitrogen functions in both catalyst samples. This may also promote the performance of the catalysts towards ORR. To further consolidate the TEM data, XPS results also reveal the chemical state of Fe element. The XPS spectra fig. 13 and 14 show Fe 2P which can be deconvoluted into three peaks at 709.2 eV, 710.6 eV and 723.1 eV for Fe-N-C/ketjenblack and Fe-N-C/Vulcan. The photoelectrons peak at 709.2 eV is attributed to Fe-N (FeN_2 & FeN_4), 710.6 eV is corresponding to the binding energy of $2P_{3/2}$ of Fe^{3+} while the peak at 723.1 eV corresponds to $2P_{1/2}$ of Fe^{2+}. The heat treatment may cause Fe to be anchored into the carbon matrix forming iron nanoparticles which could also contribute to oxygen reduction reaction

activity. Formation of Fe-N$_X$ moieties may not be rule out as XPS did reveal the formation of such nitrogen functions in the two catalysts.
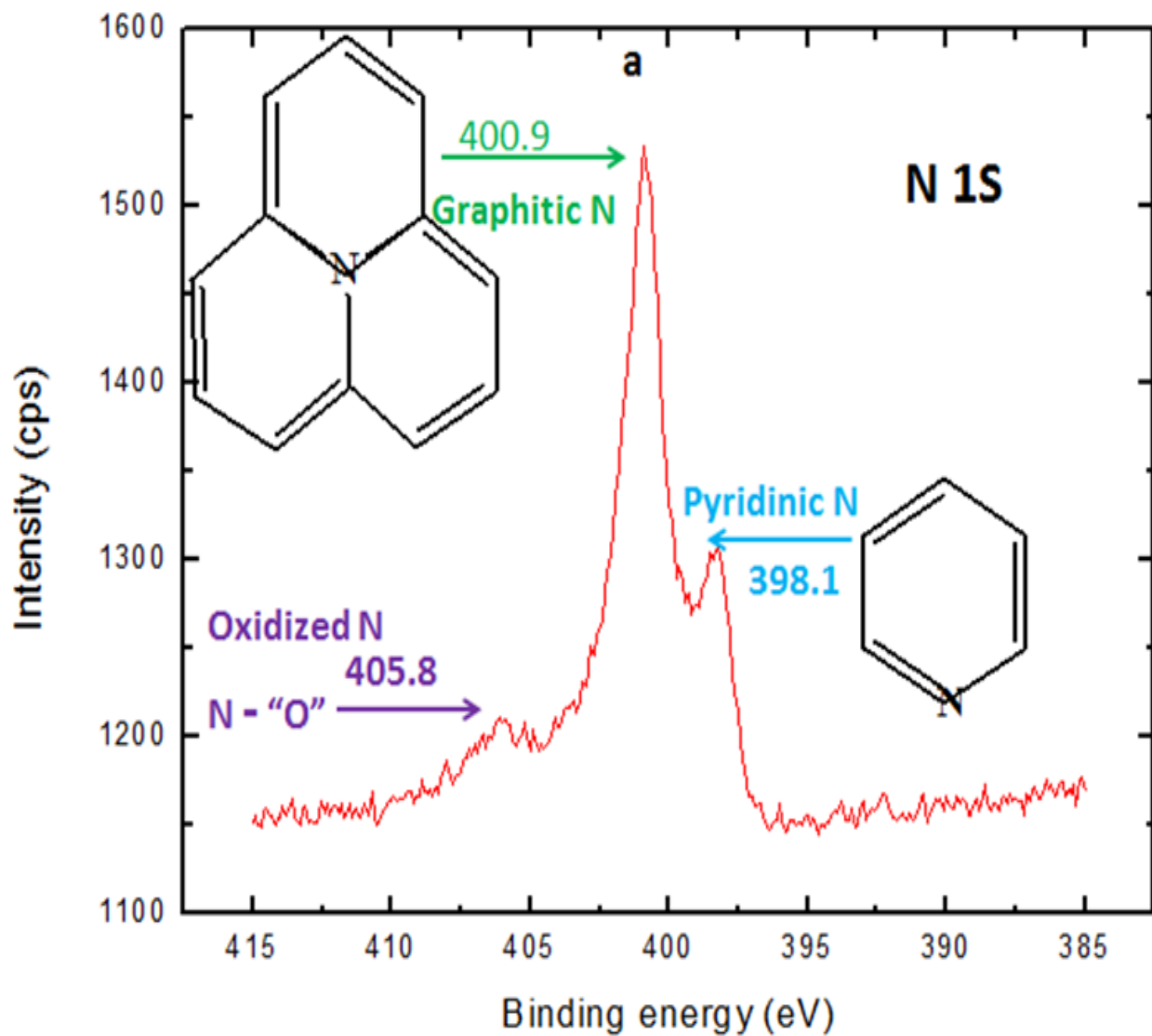

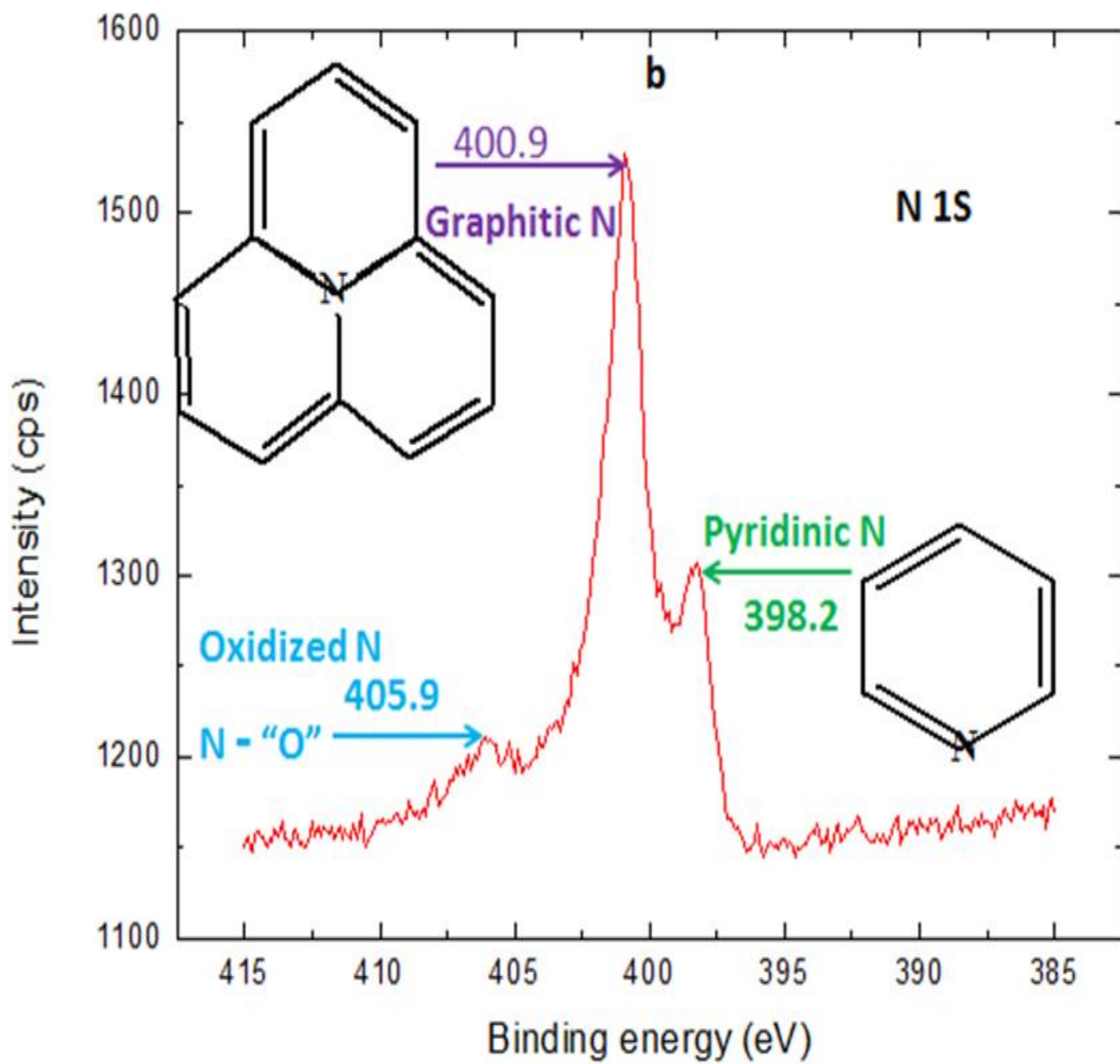Figure 9: XPS spectrum showing the three main peaks of N1S of Fe-N-C/Ketjenblack

Figure 10: XPS spectrum showing the three main peaks of N1S of Fe-N-C/Vulcan
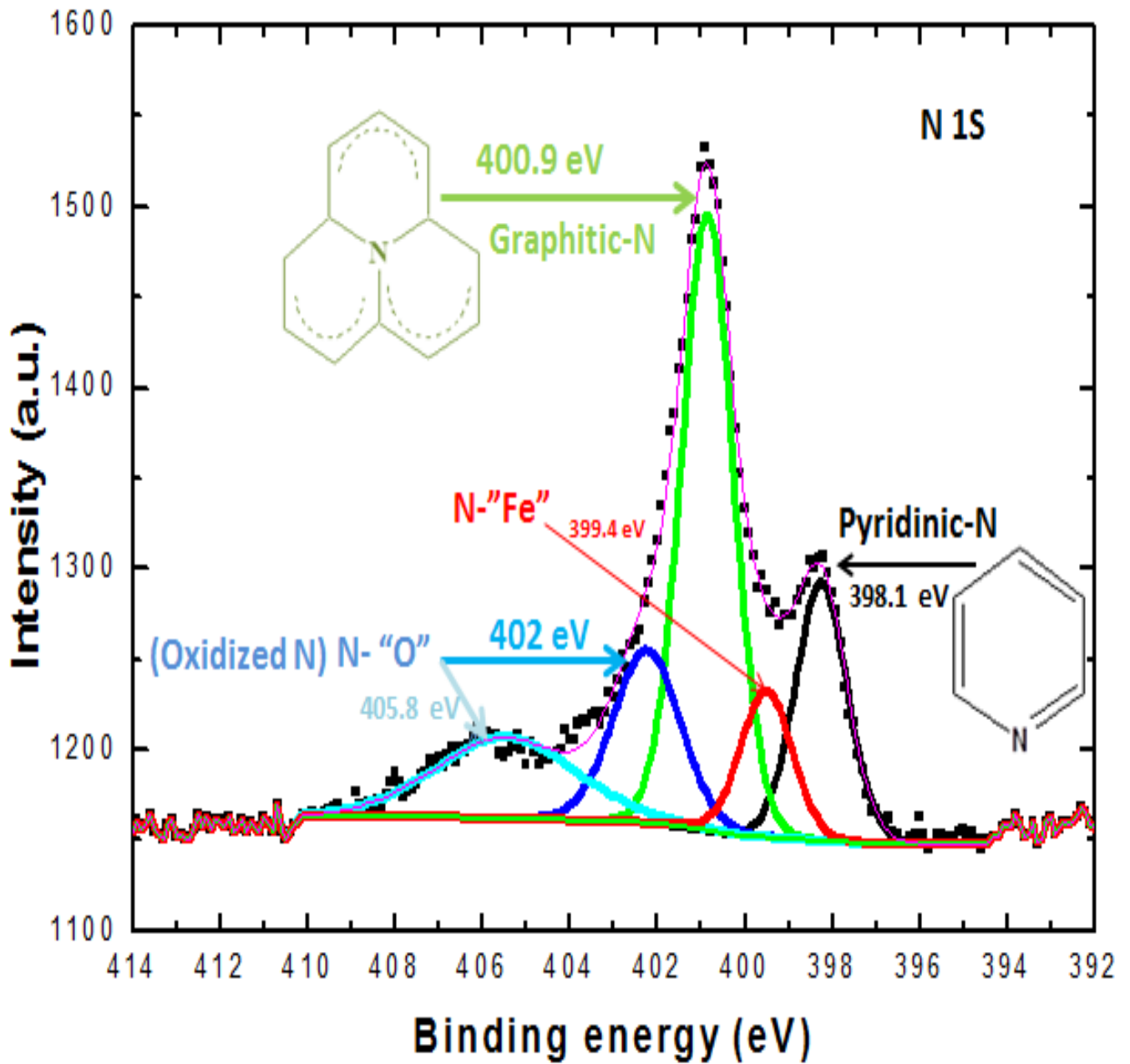
Figure 11: XPS Deconvoluted peaks showing additional two shoulder peaks with the three main peaks of N 1S spectrum of Fe-N-C/ketjenblack.
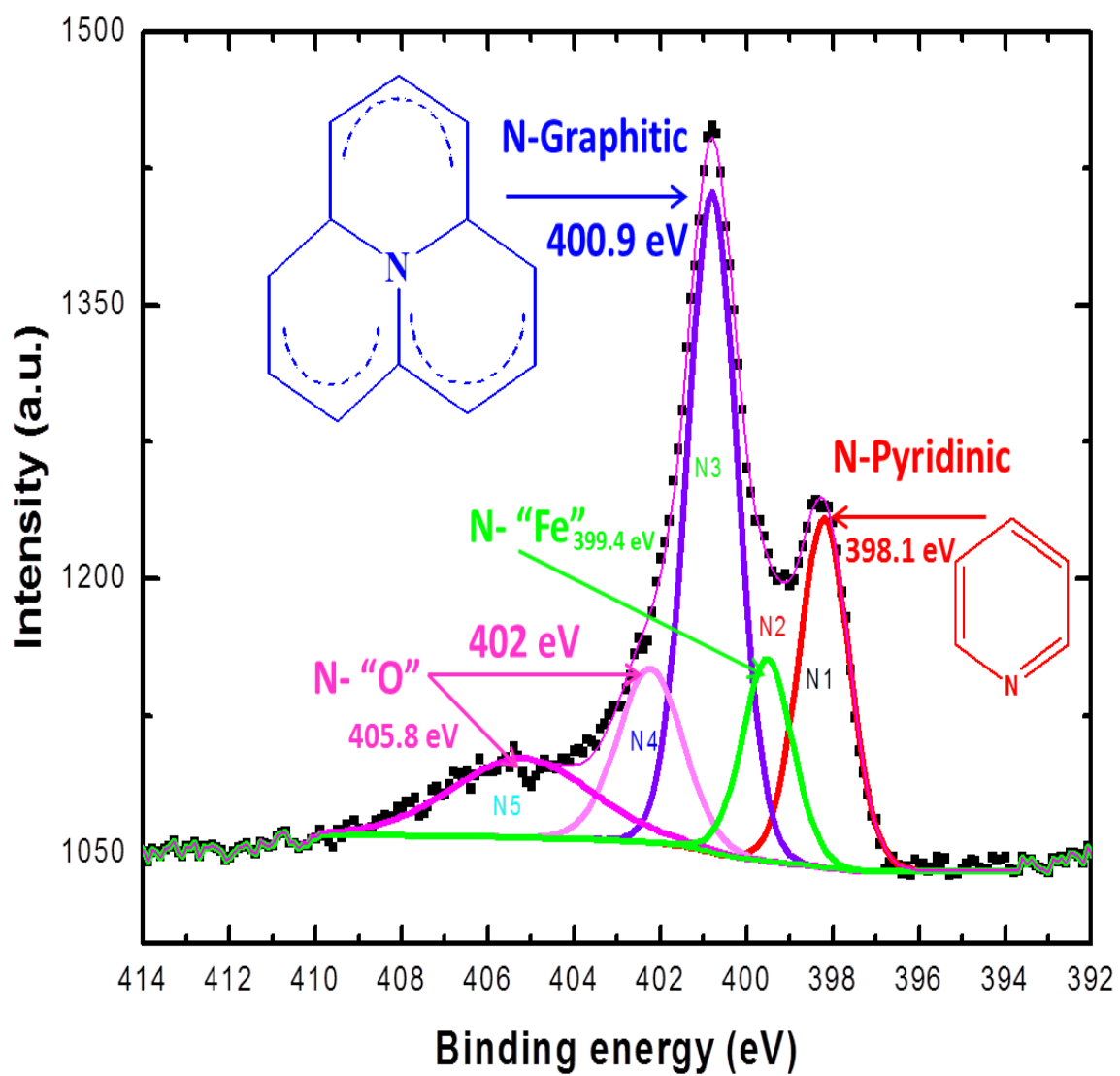
Figure 12: XPS Deconvoluted peaks showing additional two shoulder peaks with the three main peaks of N 1S spectrum of Fe-N-C/Vulcan.
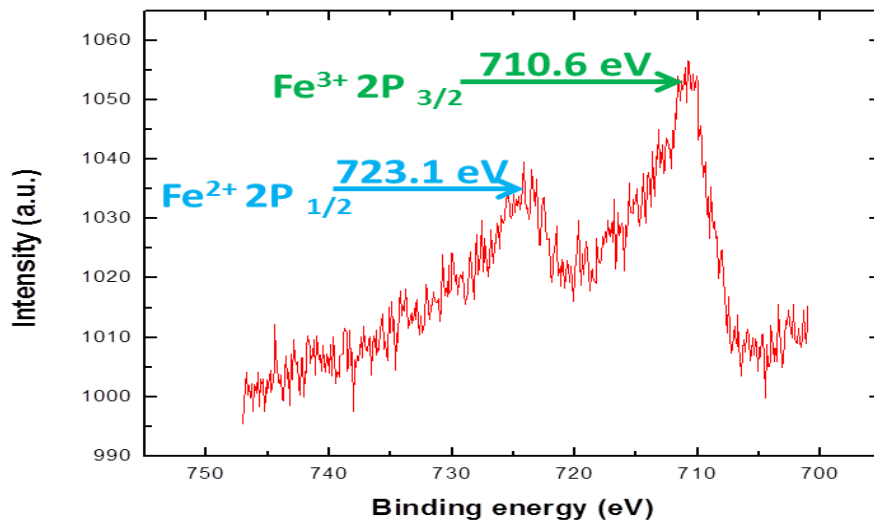
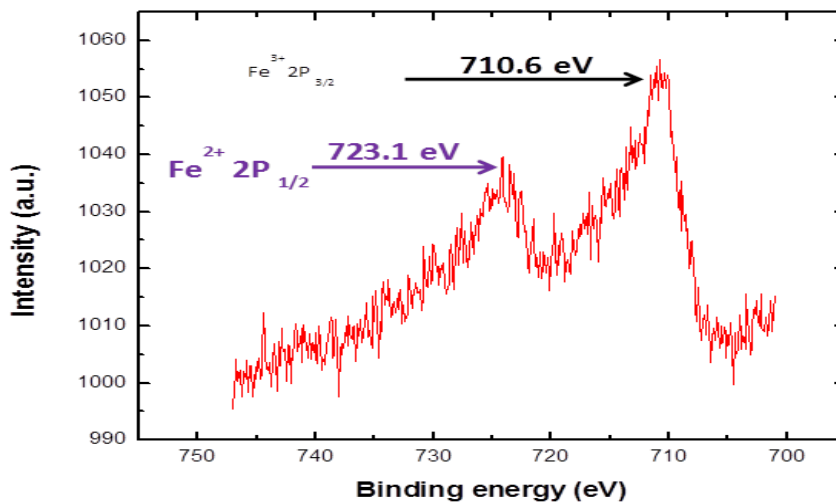Figure 13: XPS spectrum of Fe 2P of Fe-N-C/Ketjenblack

Figure 14: XPS spectrum of Fe 2P of Fe-N-C/Vulcan

4.1.7 BET AREA

The BET area measurements were conducted using ASAP-220 physisorption Analyzer from micrometrics. The BET area of all raw carbon supports were measured as well as the synthesized catalysts (Table 4). All the synthesized catalysts except Fe-N-C/KB show increase in BET area. This might be due to its initial high surface area of the raw carbon. The increase in BET area may be due to degasification such as; CO_2, Cl_2, and HCl during heat treatment and this might be responsible for the formation of active sites that resulted to an improved oxygen reduction as revealed by XPS.

Raw Carbon	BET Area(m^2/g)	Catalyst	BET Area(m^2/g)
Ketjenblack	800	Fe-N-C/KB	508.6
Vulcan	254	Fe-N-C/Vulcan	588.8
CNT	170	Fe-N-C/CNT	323.8
Acetylene black	60	Fe-N-C/ACB	407.4

Table 4. BET areas of the raw carbon supports and as- synthesized catalysts.

4.2 Electrochemistry Characterization

The electrochemical behaviors of obtained catalysts, both their stability and catalytic activities for the oxygen reduction reaction were investigated using a thin film rotating disk electrode. A typical three-electrode glass cell was used for this work as shown in the fig. 11 below.
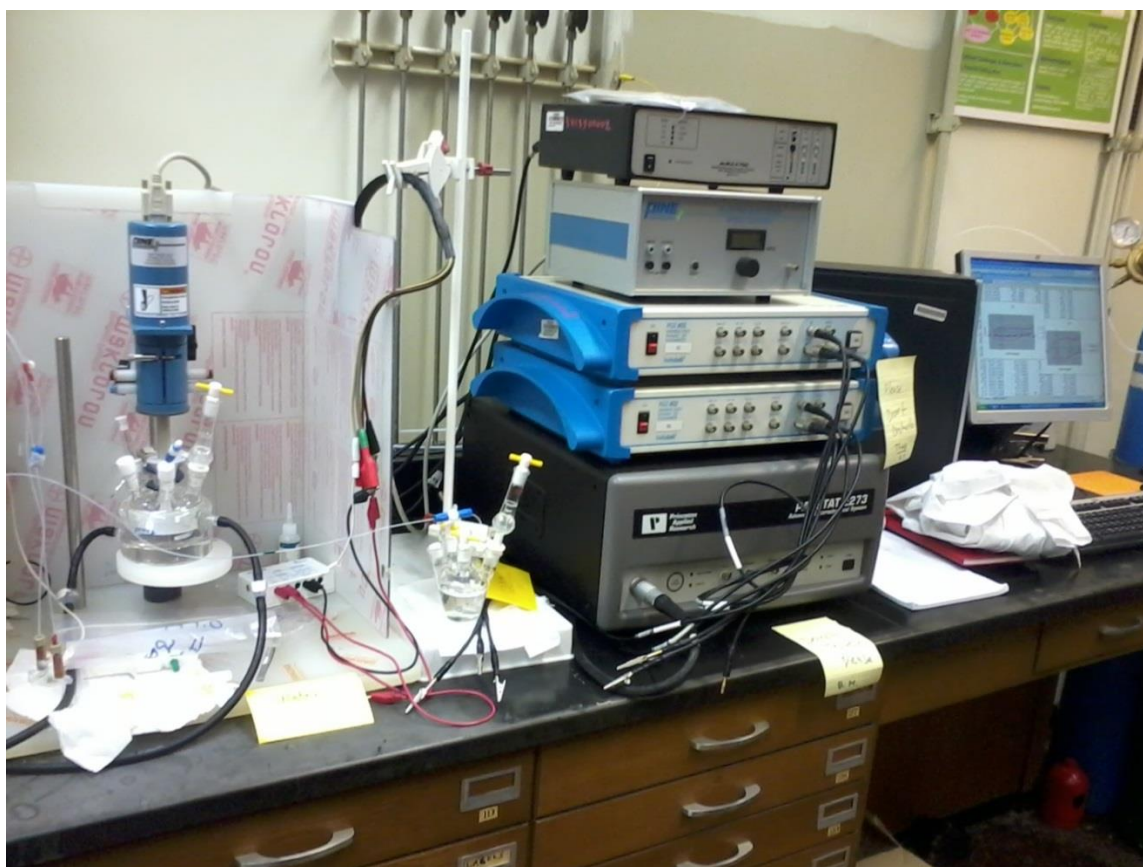

Figure 15: A laboratory set-up for electrochemical measurement

4.2.1 Electrode Preparation

For ORR activity measurement, approximately 5 mg of the dried catalyst Fe-N-C/x (x=KB, Vulcan, CNT, ACB) was dispersed in a mixture of water and isopropanol alcohol (30%

V/V) and 37µl of 1.66 % wt. Nafion® (prepared from 5% wt., Aldrich). The mixture was ultra-sonicated for 10 to 20 minutes to obtain a uniform ink. Then, 16µl of the ink suspension was deposited on the pre-cleaned glassy carbon substrate (Pine Instruments) and allowed to dry under air flow as shown in the fig. 12 below. The loading operation was repeated until the desired catalyst loading, $0.6mg/cm^2$ used for comparison during this study was achieved.

Figure 16: Thin film electrode preparation

4.2.2 Cyclic Voltammogram in N_2 saturated solution

Prior to oxygen reduction reaction measurements, each electrode was potential cycled in nitrogen saturated $0.1MHClO_4$ and 0.1MKOH for 15-20 cycles at 20mV/s until a stabilized cyclic Voltammogram (CV) was recorded. It shows a capacitive envelope between 0 and 1.2V/RHE with a pair of wide redox peaks which are almost symmetrical at 0.8V/RHE. Fig 17(a, b) shows the CV obtained for all the four catalysts obtained in 0.1M $HClO_4$ and 0.1M KOH.
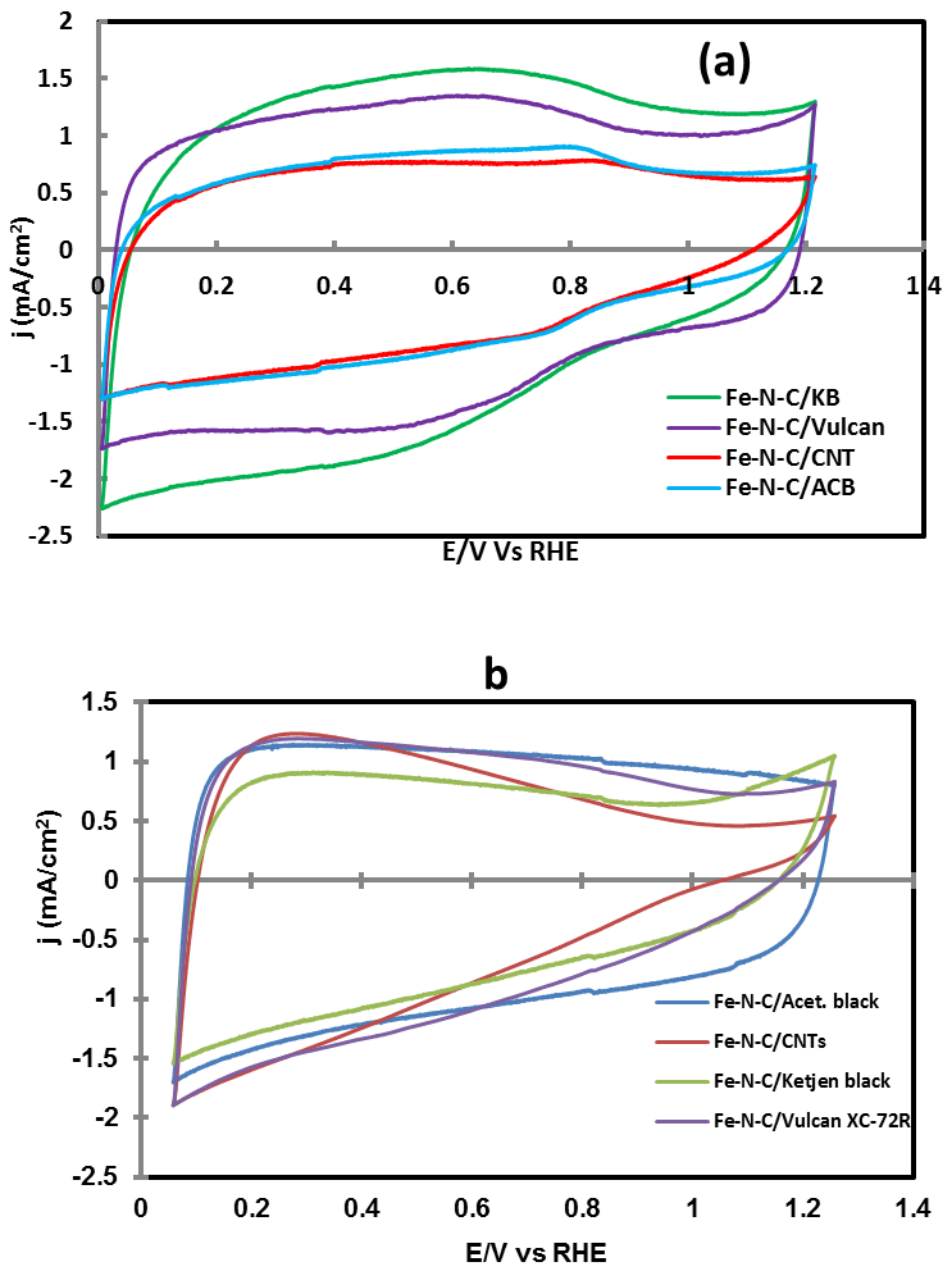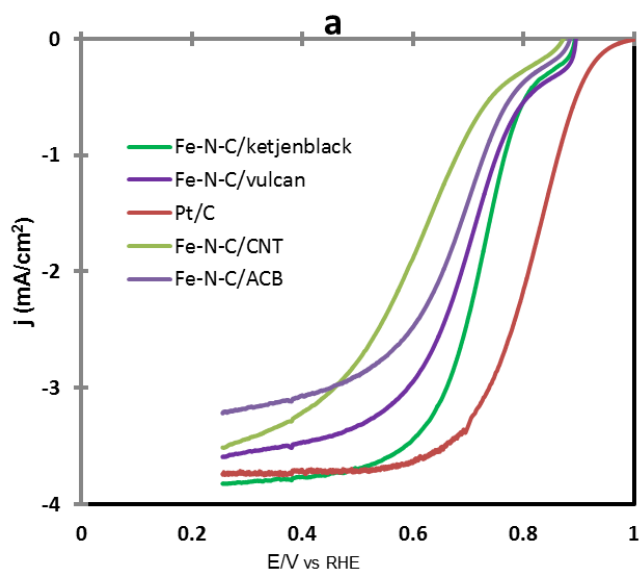
Figure 17: Voltammetry curves of the catalysts in N2-saturated obtained between 15-20 cycles (a) 0.1M HClO$_4$ and (b) 0.1M KOH

4.2.3 Effect of Carbon supports on ORR activity

To unequivocally establish the role and extent of surface area effect of carbon supports towards oxygen reduction reaction in acid and alkaline media, four carbon supports

41

(ketjenblack, Vulcan, CNT and acetylene black)   of varying surface area as given in the table 4 above were used to synthesize the catalysts. Based on the results of oxygen reduction reaction measurements, though the effect of surface area cannot be totally ruled out the determining factor for obtaining excellent ORR activity depends solely on the synthesis method used. This can be noticed in ORR activity especially in alkaline medium (fig. 14) where (Fe-N-C/Vulcan & Fe-N-C/KB) and (Fe-N-C/CNT & Fe-N-C/ACB) have comparable activity despite huge differences in surface area of the carbon supports. The synthesis method employed during this study was carefully tailored to achieve almost similar active sites irrespective of the carbon support used as revealed by XPS analysis.
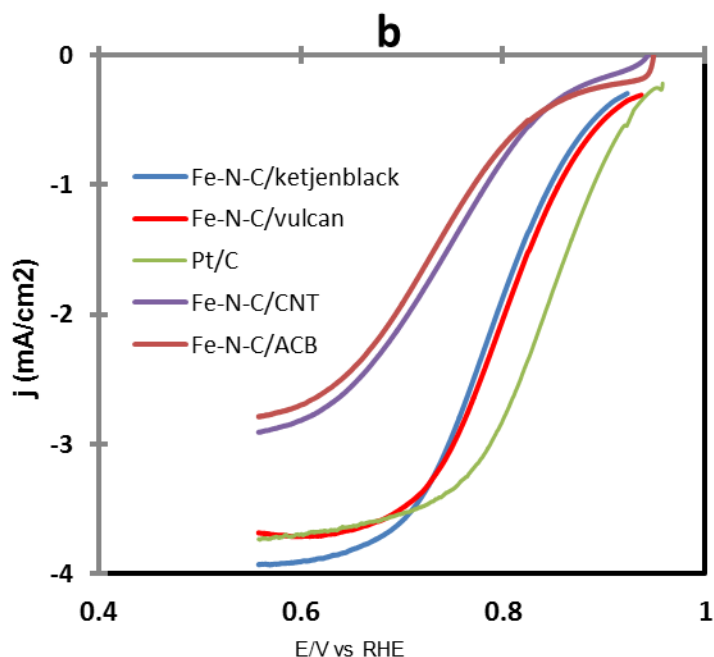
Figure 18: RDE polarization curves obtained for Fe-N-C/X (X= KB, Vulcan, CNT and ACB) and Pt/C in O_2 saturated (a) 0.1M $HClO_4$ and (b) 0.1M KOH

To understand the kinetics of the synthesized catalysts towards ORR, linear sweep voltammetry measurements were conducted on RDE in 0.1M $HClO_4$ and 0.1M KOH (oxygen saturated) at 900rpm with a scan rate of 5mV/s and compared to that of Pt/C (25μg/cm^2) as shown in Fig. 14 above . The corresponding onset potentials and half-wave potentials in 0.1MHClO4 and 0.1MKOH of the catalysts were presented in table 5 below. For our best catalyst, Fe-N-C/ketjenblack, the half-wave potential was only 78mV and 30 mV lower than that of Pt/C in acidic and alkaline media respectively.

Catalyst	0.1M HClO$_4$		0.1M KOH	
	E$_{onset}$/V	E$_{1/2}$/V	E$_{onset}$/V	E$_{1/2}$/V
Fe-N-C/KB	0.85	0.73	0.95	0.802
Fe-N-C/Vulcan	0.86	0.732	0.95	0.82
Fe-N-C/CNT	0.84	0.62	0.92	0.76
Fe-N-C/ACB	0.84	0.69	0.92	0.75
Pt/C	0.95	0.81	0.96	0.832

Table 5. Summary of the half-wave and Onset potentials in 0.1M HClO4 and 0.1M KOH

4.2.4 Effect of Catalyst loading on ORR activity

The oxygen reduction activity of Fe-N-C/x (x=KB, Vulcan, CNT and ACB) was evaluated in an oxygen saturated 0.1MHClO4 and 0.1MKOH solutions with catalyst loadings of 0.2mg/cm^2, 0.4mg/cm^2 and 0.6mg/cm^2. The polarization curves obtained are shown in figure 15 and 16 in acidic and alkaline media respectively. It can be seen that the current densities are increased with increasing catalyst loading, and the ORR on-set potentials have no significant change with catalyst loading. Though, at low catalyst loading the limiting currents were not ill- defined but became better as the catalyst loading was increased due to more active sites for oxygen reduction. From such high activity obtained during this work especially with Fe-N-C/KB and Fe-N-C/Vulcan it could be that oxygen reduction reaction proceeds through a 4- e$^-$ transfer process especially at higher catalyst loading.
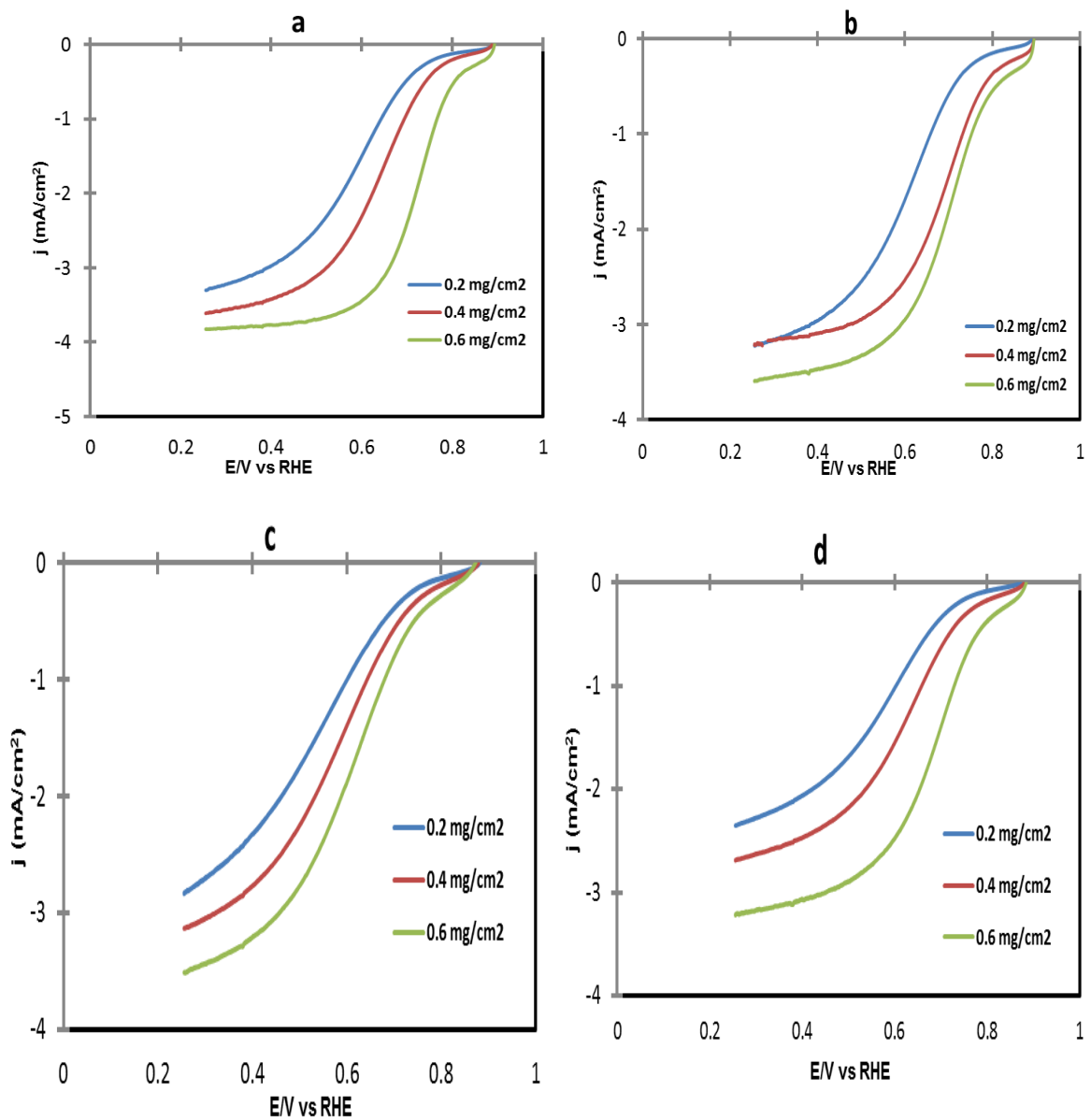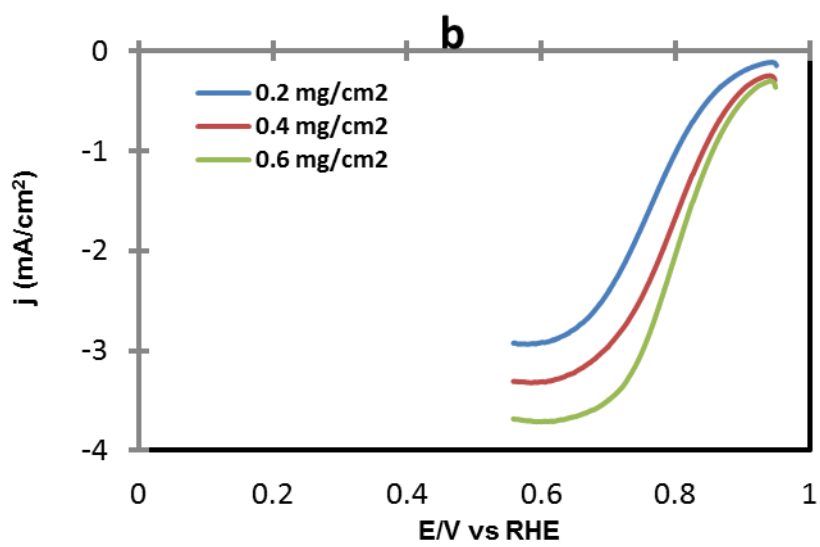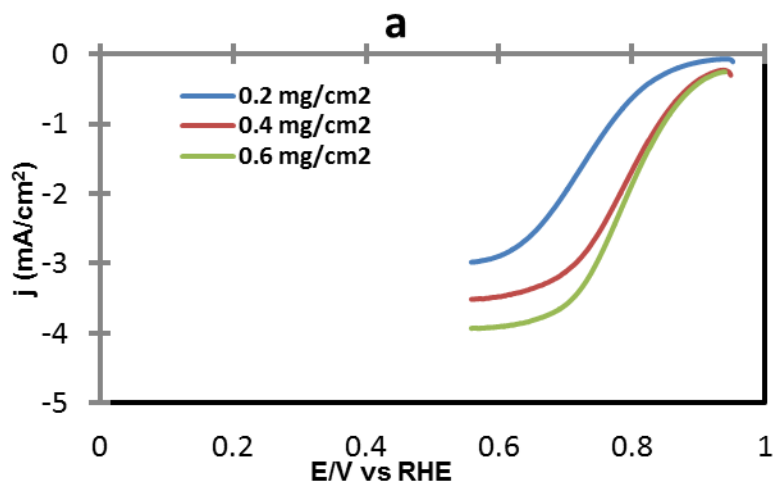
Figure 19 Catalyst loading effect on ORR in 0.1M HClO$_4$ (a) Fe-N-C/KB (b) Fe-N-C/Vulcan (c) Fe-N-C/CNT and (d) Fe-N-C/ACB
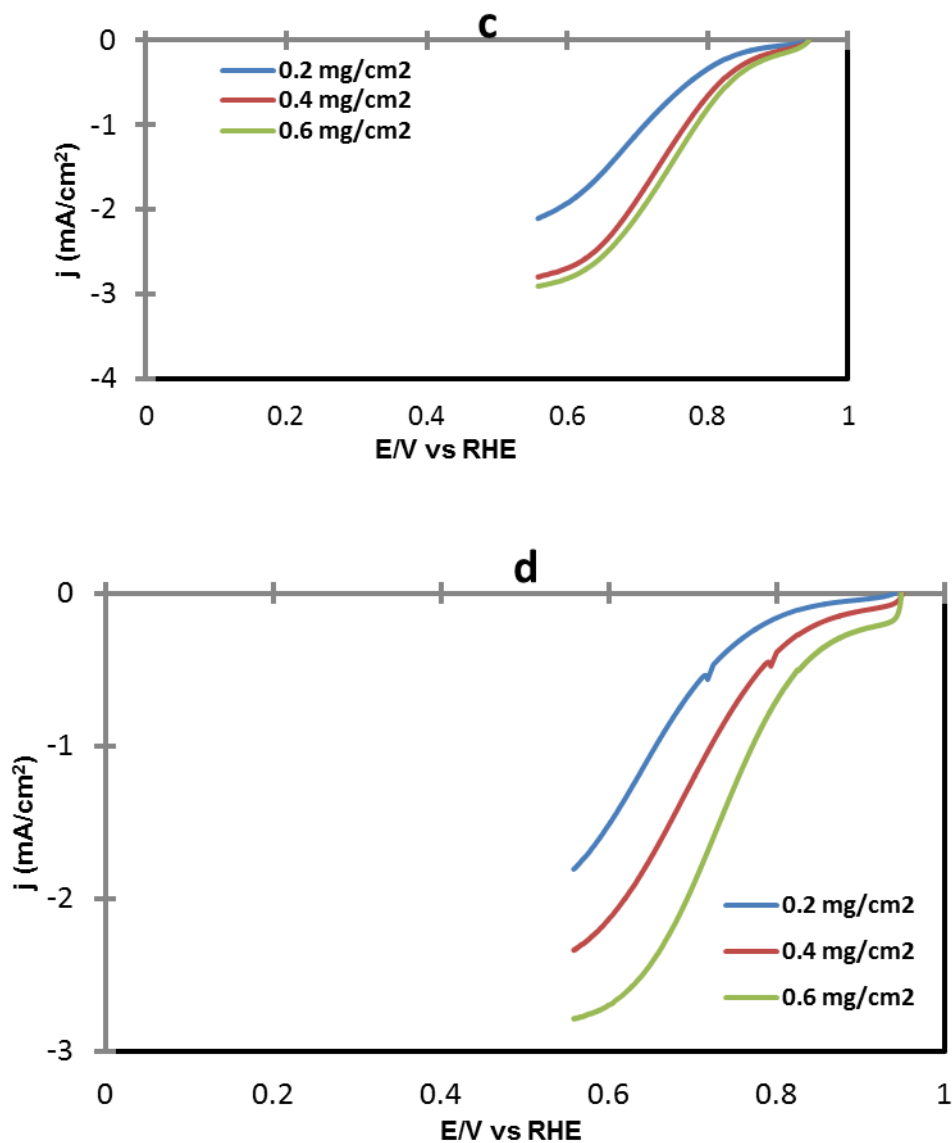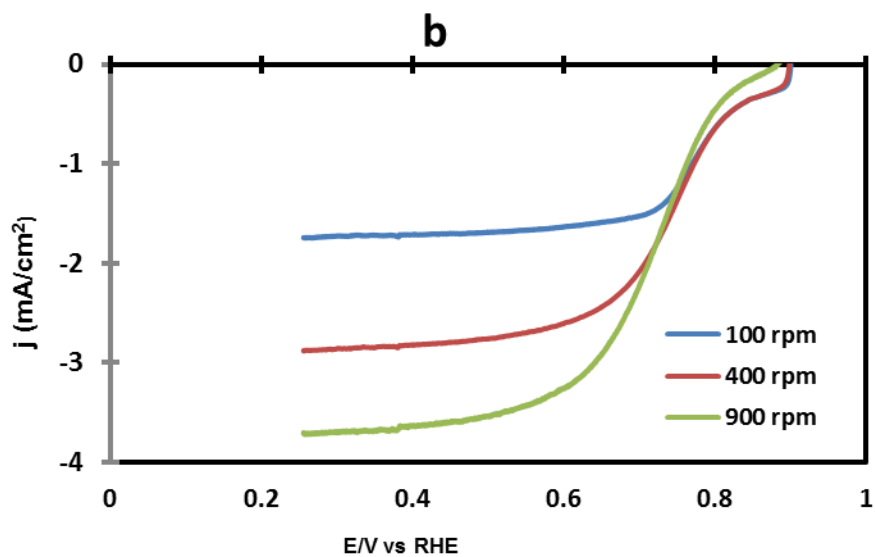
Figure 20: Catalyst loading effect on ORR activity in 0.1MKOH (a) Fe-N-C/KB (b) Fe-N-C/Vulcan (c) Fe-N-C/CNT and (d) Fe-N-C/ACB

4.2.5 Effect of Rotation speed on ORR activity

Fig. 17 and 18 show the polarization curves obtained for the various rotation speed, 100, 400 and 900 rpm of RDE on ORR for the catalyst loading, 0.6 mg/cm^2 in 0.1M HClO4 and 0.1M KOH medium respectively. It is well known that more active sites of the catalyst are

brought to the disk of RDE for the oxygen reduction reaction at higher speed which implies high ORR activity.

Figure 21: Rotation speed effect on ORR activity in 0.1M HClO$_4$ (a) Fe-N-C/KB (b) Fe-N-C/Vulcan (c) Fe-N-C/CNT and (d) Fe-N-C/ACB
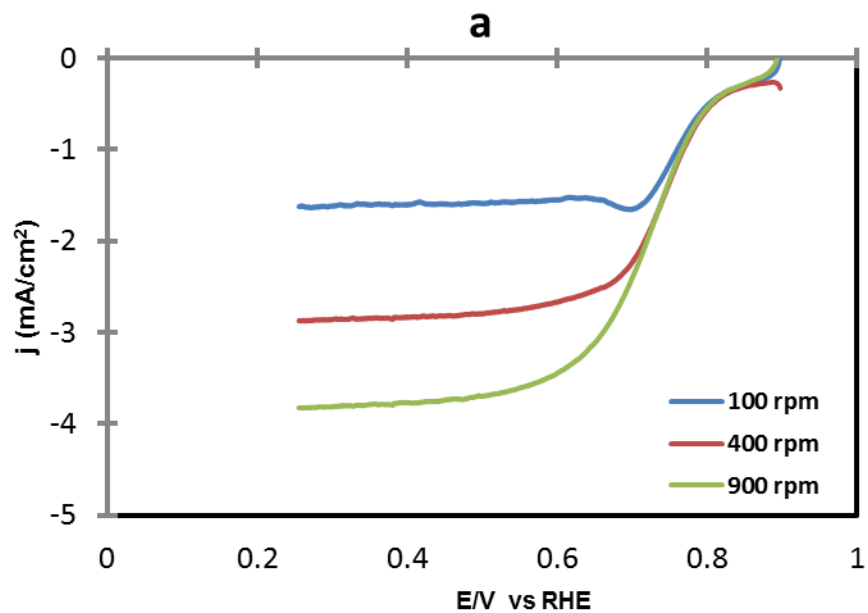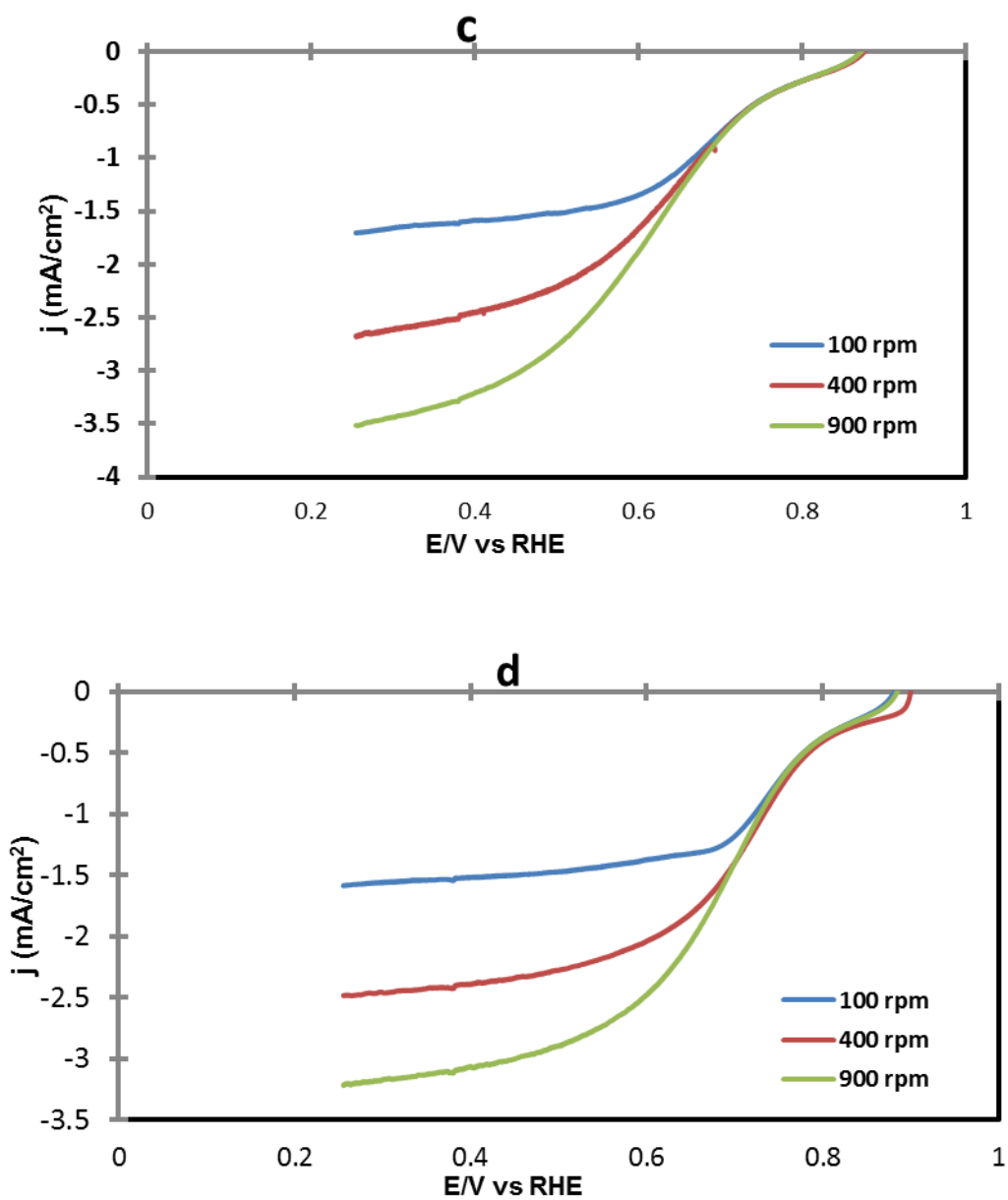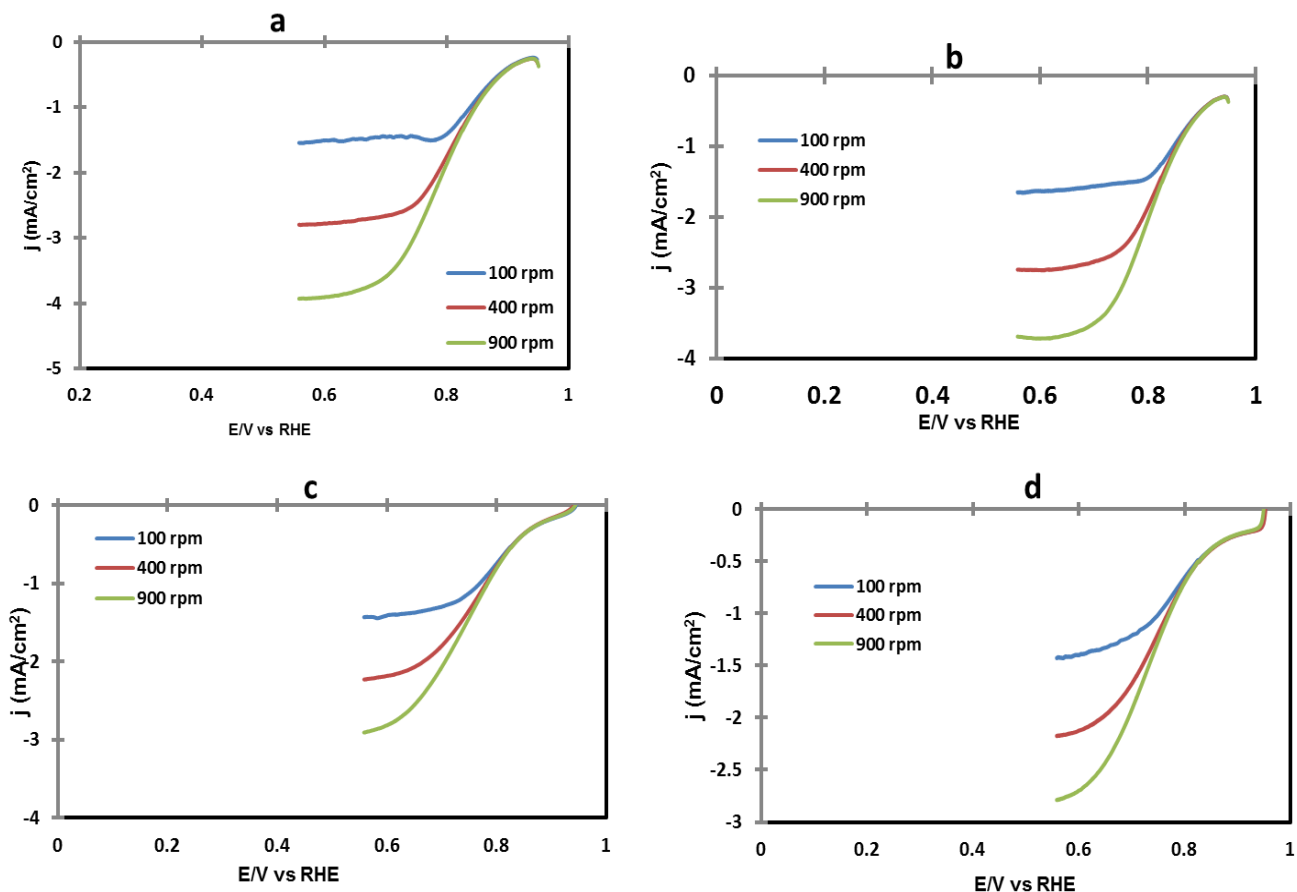
Figure 22: Rotation speed effect on ORR activity in 0.1M KOH (a) Fe-N-C/KB (b) Fe-N-C/Vulcan (c) Fe-N-C/CNT and (d) Fe-N-C/ACB

4.2.6 Methanol Tolerance

The catalysts synthesized through this new synthesis method also show remarkable methanol tolerance even at high concentration of 0.5M CH_3OH in both acidic and alkaline media fig. 19 and 20 respectively. Furthermore, chronoamperommetry test was also conducted at a potential hold of 0.8V/ RHE for 15 minutes in alkaline medium in the presence of 0.5M CH_3OH. As it can be seen in fig. 21, a significant drop in activity was

50

observed for Pt/C, whereas Fe-N-C/Vulcan did not undergo any change in electrode performance. Synthesizing a catalyst that has high ORR activity, stability and at the same time being tolerance to methanol is a challenge. Pt-based catalysts may not be the right candidates for direct methanol Fuel cells (DMFCs) due to cross-over of methanol through the polymer membrane electrolyte. Non precious metal based catalysts (especially nitrogen doped carbon) have proven to serve as alternative to Pt because of their excellent tolerance to methanol.

Figure 23: Methanol tolerance in 0.1M $HClO_4$ (a) Fe-N-C/KB (b) Fe-N-C/Vulcan (c) Fe-N-C/CNT and (d) Fe-N-C/ACB, 5mV/s, 900 rpm, RT, 0.6 mg/cm^2
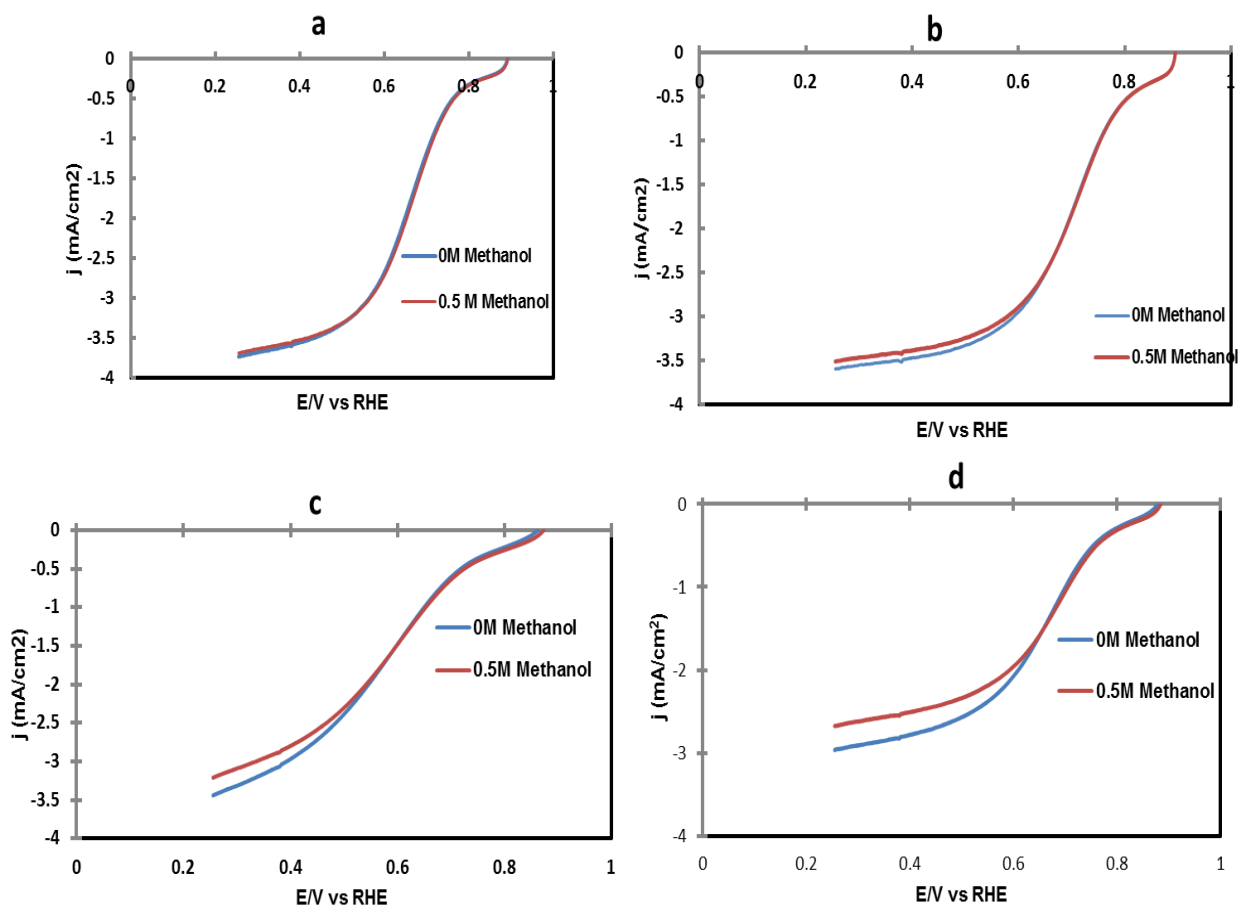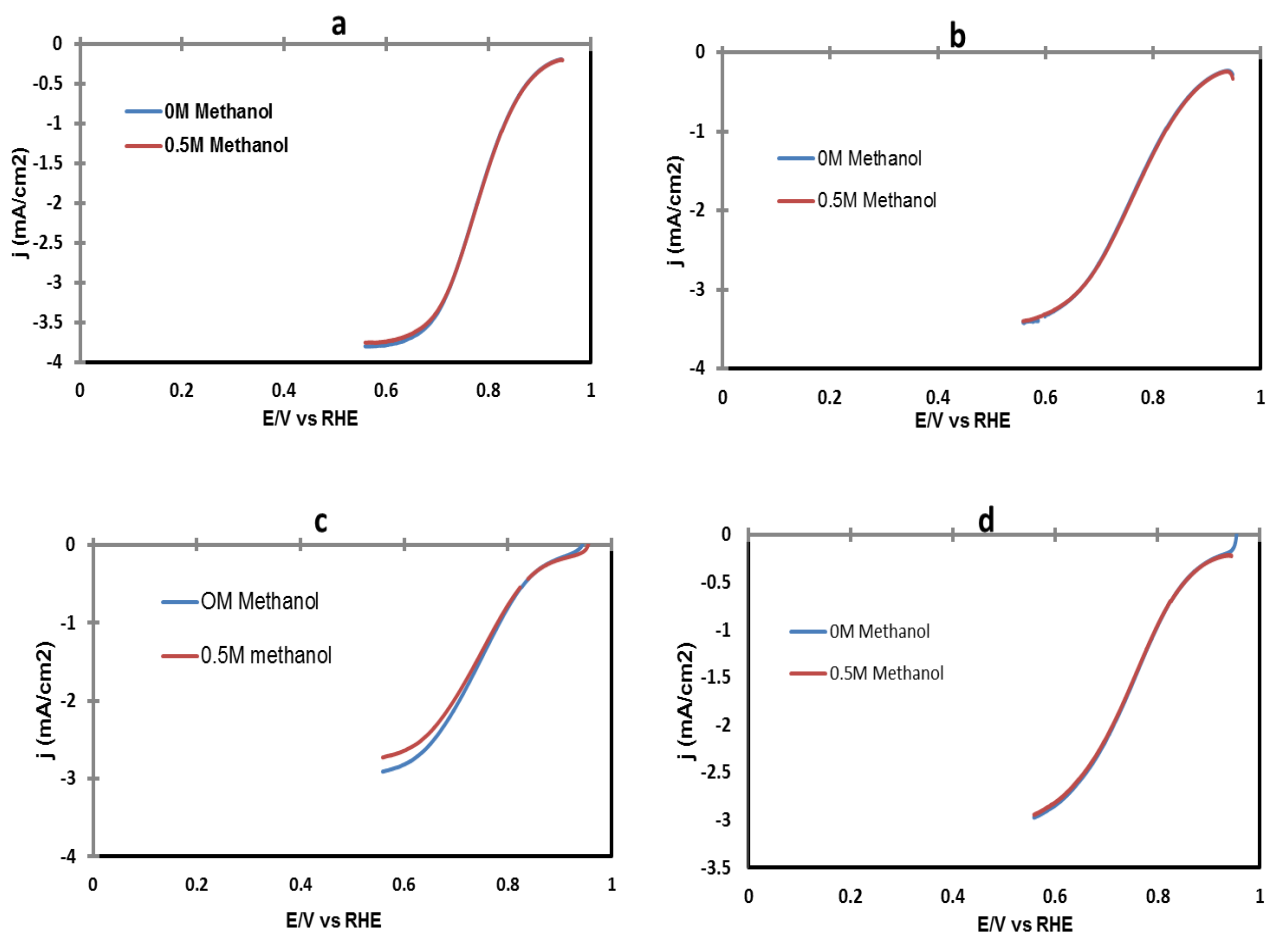
Figure 24: Methanol tolerance in 0.1M KOH (a) Fe-N-C/KB (b) Fe-N-C/Vulcan (c) Fe-N-C/CNT and (d) Fe-N-C/ACB, 5mV/s, 900 rpm, RT, 0.6 mg/cm^2
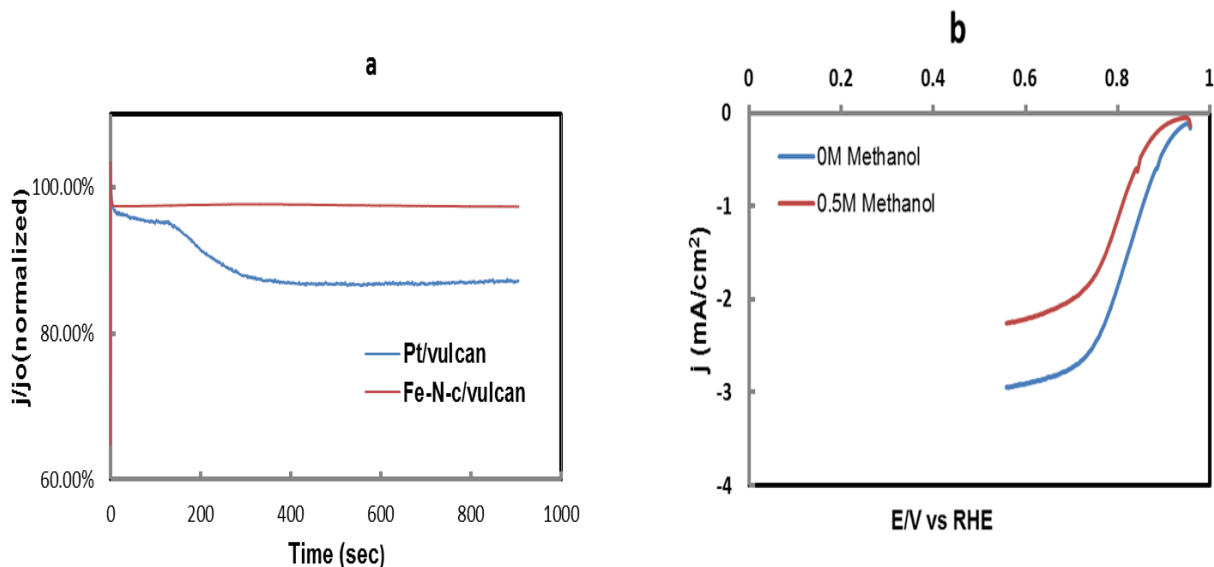
Figure 25: Chronoamperommetry curve (CA) in O_2 saturated 0.1M KOH establishing Fe-N-C/Vulcan methanol tolerance as compared to that of Pt/Vulcan. 5 mV/s, 900 rpm, RT 0.5M CH_3OH, 0.8 V potential hold. (b) RDE methanol tolerance for Pt/Vulcan

4.2.7 Durability Test

In real fuel cell operation condition, cathode catalyst stability still remains a factor impeding fuel cell commercialization for all Pt-based and non-Pt based materials. This prompted us to carry out a prolong durability study on our promising catalysts obtained through this new synthesis approach. The durability test was investigated by chronoamperommetry experiments in oxygen saturated 0.1M $HClO_4$ and 0.1M KOH between 0.65 and 1.0V/RHE for 15, 000 cycles using a square wave signal of 5s at each potential. Durability test was carried out in a separate electrochemical cell designated for such use. The ORR activities of the cycled catalysts were measured in a fresh electrolyte after every 5,000 cycles. To our ultimate surprise, activity gains were observed in only acidic medium for the first 10k cycles. This may be due to full catalyst utilization as a result

of cycling. The cyclic voltammetry curves obtained after stability test in 0.1 MHClO4 and 0.1M KOH are given in fig. 22 and 23 respectively for the best two catalysts.
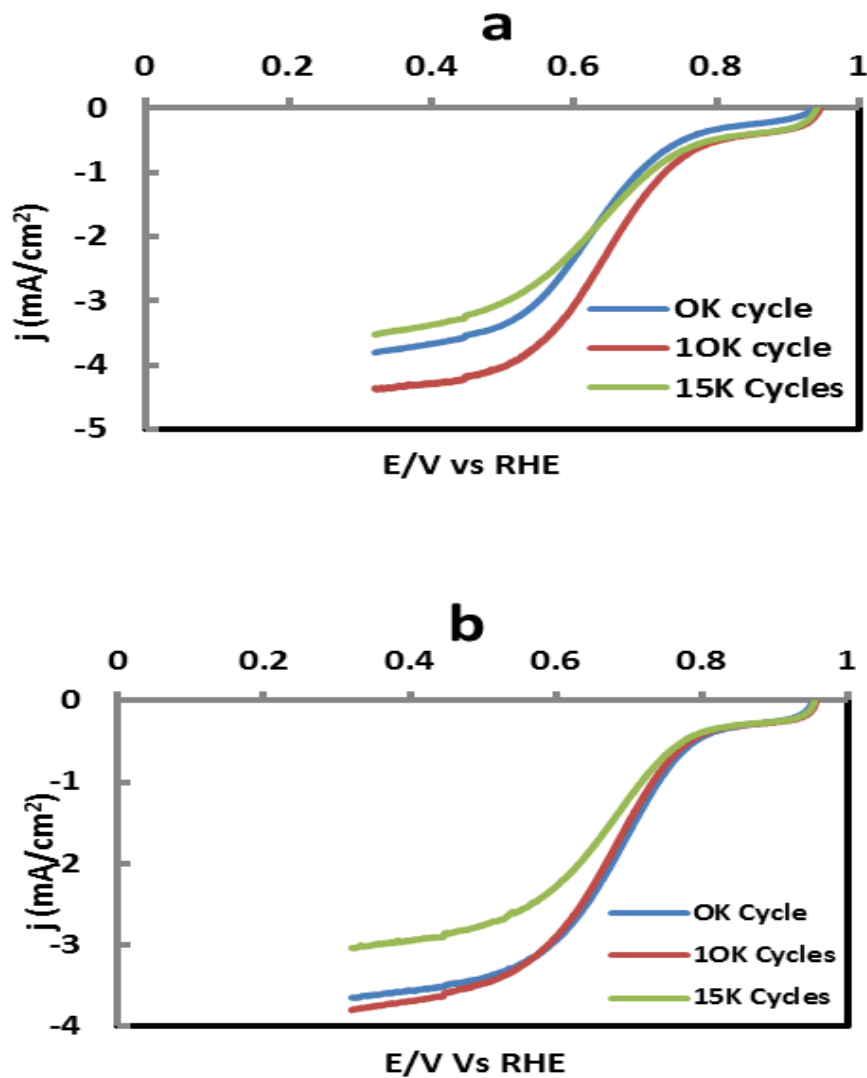

Figure 26: Voltammetry curves in O_2 saturated 0.1M $HClO_4$ (a) Fe-N-C/ketjenblack (b) Fe-N-C/Vulcan, 5 mV/s, 900 rpm, and room temperature.
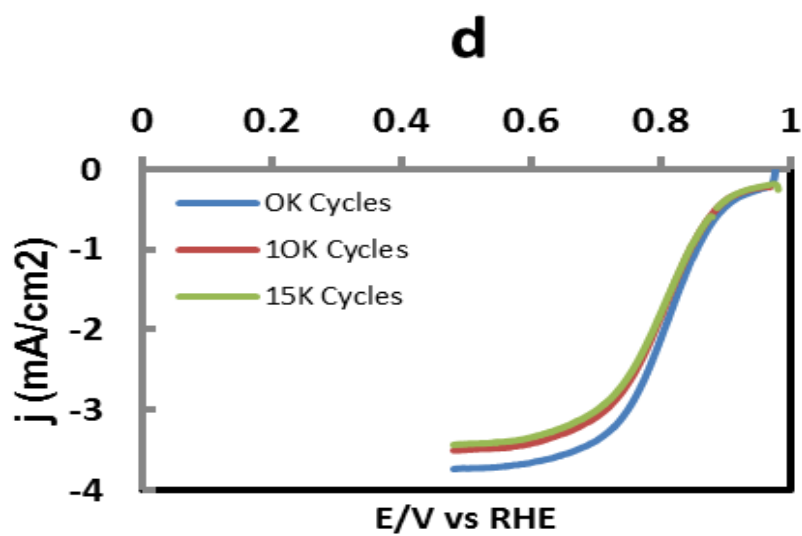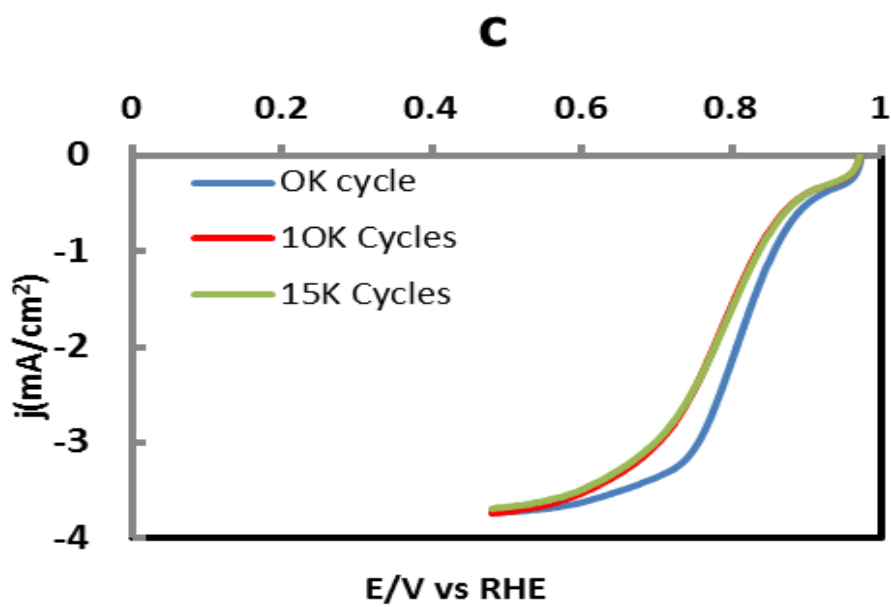
Figure 27: Voltammetry curves in O_2 saturated 0.1M KOH (c) Fe-N-C/ketjenblack (d) Fe-N-C/Vulcan, 5 mV/s, 900 rpm, and room temperature.

4.2.8 Electron transfer number as analyzed by Koutechy-Levich Principle

The RDE polarization curves obtained were analyzed by Koutechy-Levich principle (fig. 24) for both acidic and alkaline media by means of equations 1 and 2 below:

$$1/j = 1/j_k + 1/j_{lim} \quad .... \quad (eq\ 1)$$

$$= 1/nFC_{O2}K_{O2}\Gamma \quad + \quad 1/0.62nFC_{O_2}D_{O_2}^{2/3} V^{-1/6}w^{1/2} \quad ………………………………. \quad (eq\ 2)$$

The apparent number of electrons transferred (n) were extracted from the slope. j= measured current density j_k= kinetic current density j_{lim}= limiting current density F= faraday's constant (96485 $Cmol^{-1}$) C_{O2}= concentration of oxygen (1.26 x 10^{-6} mol/cm^3) in $0.1MHClO_4$ and 1.2 x10^{-6} in 0.1M KOH mol/cm^3) K_{O2}= kinetic rate constant for the catalyzed ORR (cm^2s^{-1}) Γ = total surface coverage of the catalyst (mol/cm^2) D_{O2}= diffusion coefficient of oxygen in aqueous solution (in $0.1MHClO_4$ 1.93 x10^{-5} and 1.9 x 10^{-5} in 0.1MKOH cm^2s^{-1}) V= kinematic viscosity (0.01009 in $0.1MHClO_4cm^2s^{-1}$) and W= rotation speed of the electrode ($rads^{-1}$) [41, 42].
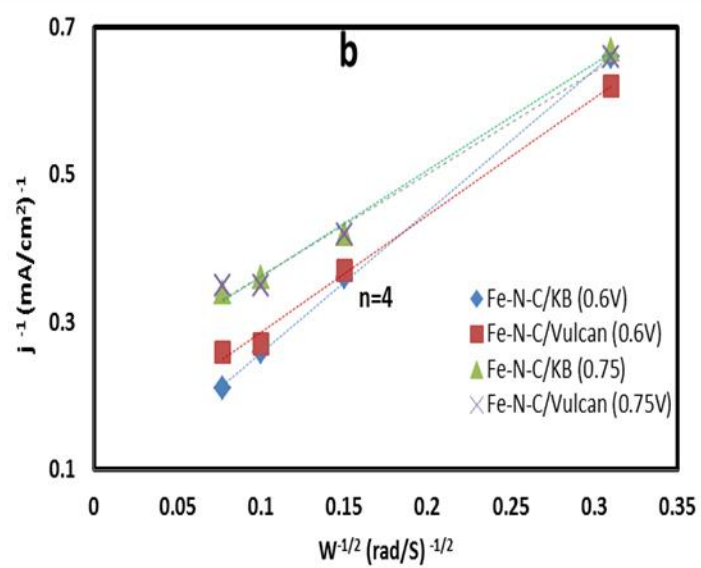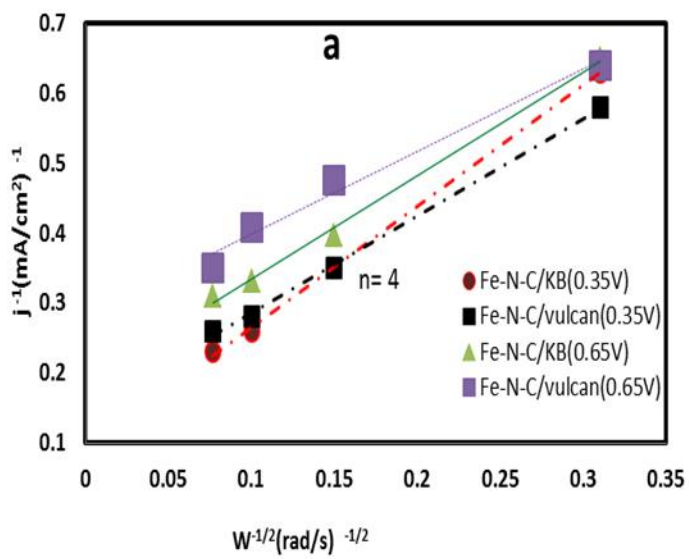
Figure 28: Koutechy-Levich plots obtained from RDE voltammetry curves recorded at different rotation speed (a) 0.1M $HClO_4$ and (b) 0.1M KOH

From fig. 24 above, the results indicate an ORR proceeds via a four electron transfer process.

Acidic Medium

$O_2 + 4H^+ + 4e^- \longrightarrow 2H_2O$

$O_2 + 2H^+ + 2e^- \longrightarrow H_2O_2$

$H_2O_2 + 2H^+ + 2e^- \longrightarrow 2H_2O$

Alkaline Medium

$O_2 + 4H_2O + 2e^- \longrightarrow HO_2^- + OH^\bullet$

$O_2 + H_2O + 4e^- \longrightarrow 4HO^\bullet$

$HO_2^- \longrightarrow HO^-$

$HO_2^- \longrightarrow HO^\bullet + [O_2]$

$HO^\bullet + HO^- \longrightarrow H_2O_2$

$H_2O_2 + 2e^- \longrightarrow H_2O$
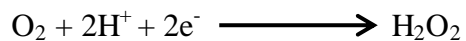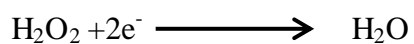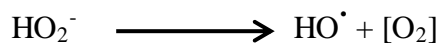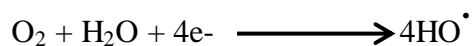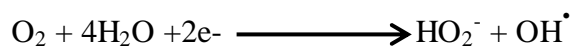
Scheme 5: Proposed mechanism for oxygen reduction

CONCLUSION

This thesis was carried out successfully and the following scientific contributions to the literature are some of its outcomes:

1. Fe-N doped Carbon was successfully synthesized by polymerizing aniline salt on a carbon support using newly developed aqueous $Fe3^+/H_2O_2$ catalytic system as a new oxidant.

2. The newly developed synthesis method has proven well to be a means of obtaining nitrogen modified carbon catalysts with desirable catalytic properties as confirmed by RDE measurements.

3. The newly developed aqueous Fe^{3+}/H_2O_2 catalytic system could replace the common use of ammonium peroxydisulfate (APS) in the literature owing to the difficulties that may arise from the removal of its reaction products.

4. Aniline salt has demonstrated better processability than liquid aniline from toxicity point of view and also its high solubility in water without any additive.

5. High surface area of carbon support does not mean high ORR activity but the synthesis method plays a key role for obtaining high active sites for ORR.

The development of Nitrogen doped carbon catalysts through application of Fe^{3+}/H_2O_2 and aniline salt unfolded the following product development niches:

1. Environmentally friendly means of obtaining nitrogen doped carbon catalyst with excellent oxygen reduction reaction activity as confirmed by RDE electrochemical technique.

2. Stability in both acidic and alkaline media have been achieved expanding the wider application of the catalysts to include PEMFC and AFC

3. Remarkable methanol of the catalysts also suggesting their application usage in DMFC.

4. Probable means of obtaining high graphitic-N active site which is most required for high ORR activity and stability for nitrogen doped carbon catalysts was achieved.

RECOMMENDATIONS

The following are recommended for future work

1. Aniline can be easily polymerized with other monomers as copolymer (such as acrylonitrile, vinazene, and pyrrole) as a means of obtaining high modified doped carbon catalyst and thus suggested for future work.

2. Fuel cell real application testing of the synthesized catalyst could be further investigated.

3. Incorporation of metal oxide (e.g. tungsten oxide, titanium oxide) into catalyst which could enhance ORR activity is suggested for future work.

4. The use of environmentally friendly oxidant could be further explored to synthesize other nitrogen modified catalysts.

5. The effect of heat treatment temperature variation could be further investigated in order to establish the optimum temperature where active sites could be obtained.

REFERENCES

[1] http://www.fuelcellenergy.com/why-fuelcell-energy

[2] M. Adina, J. Pascale, J. Bruno, and P. Serge, "Phys. Chem. Chem. Phys.," 2011, 13, 21600- 21607.

[3] R. Bashyam, and P. Zelenay, Nature, 2006, 442, 63-66.

[4] J.P Dodelet, in N4-Macrocyclic Metal Complexes, ed. J.H. Zagal, F Bedioui and J.P Dodelet, springer, New York 2006, Ch. 3, pp. 83-148

[5] J.P. Dodelet in Electrocatalysts in fuel cells: A Non and Low platinum Approach, M. Shao (Ed.), springer, London, 2013.

[6] S. Gupta, D. Tryk, I. Bae, W. Aldred and E. Yeager, J. Appl. Electrochem; 1989, 19,19-27

[7] R. Jasinski, Nature 201 (1964) 1212.

[8] H. Jahnke, M. Schonborn, Comptes Rendus, Troisie`mes Journe´ es Internationales d'Etude des Piles a` Combustible, Presses Acade´miques Europe´ ennes, Bruxelles, 1969, p. 60.

[9] H. Jahnke, M. Schonborn, G. Zimmermann, Top. Curr. Chem. 61 (1976) 133.

[10] D.A. Sherson, A.A. Tanaka, S.L. Gupta, D. Tryk, C. Fierro, R. Holze, E.B. Yeager, R.P. Lattimer, Electrochim. Acta 31 (1986) 1247.

[11]   A. Van Der Putten, A. Elzing, W. Visscher, E. Barendrecht, J. Electroanal. Chem.Interfacial Electrochem. 221 (1987) 95.

[12]   A.L. Bouwkamp-Wijnoltz, W. Visscher, J.A.R. Van Veen, S.C. Tang, Electrochem.Acta 45 (1999) 379.

[13]   K. Wiesener, Electrochem. Acta 31 (1986) 1073.

[14]   N. Alonso-Vante, H. Tributsch, Nature 323(1986), 431

[15]   N. Alonso-Vante, in: W Vielstich, A. Lamm, H.A. Gastreiger (Eds), Handbook of fuel cells-fundamentals, technology and Applications, vol. 2 John Wiley& sons Ltd; WestSussex, 2003, p. 534

[16]   Akimitsu I. Shotaro, D. Shigenori M. Ken- inchiroo, Electrochemical Acta 53(2008) 5442-5450

[17]   Liangti Qu, Yong Liu, Jong-Beom B and Liming Dai (2010) ACS Nano vol 4. No 3, 1321-1326

[18]   Kim, K. S.; Zhao, Y.; Jang, H.; Lee, S. Y.; Kim, J. M.; Kim, K. S.; Ahn, J. H.; Kim, P.; Choi, J. Y.; Hong, B. H. Large-Scale Pattern Growth of Graphene Films for Stretchable Transparent Electrodes. Nature 2009, 457, 706–710.

[19]   A. Reina, Jia, X.; Ho, J.; Nezich, D.; Son, H.; Bulovic, V.; Dresselhaus, M. S.; Kong, J. Large Area, Few-Layer Graphene Films on Arbitrary Substrates by Chemical Vapor Deposition. Nano Lett. 2009, 9, 30–35.

[20]   Gang L, Xuguang L, Prabhu C, Branko N.P, (2010) Electrochemica Acta 55, 2053-2058

[21]   H.A. Gasteiger, S.S. Kocha, B. Sompalli, F.T. Wagner, Appl. Catal. B 56 (2005) 9.

[22]   Chi Wen T; Hao M.C; Ru-Shi L; Kiyotaka A; Lei Zhang, Jiujunz 2, Man-Yin L. Yu-Min P, Electrochemica Acta 56 (2011) 8734-8738

[23]   Thangavelu P; Ramaiyan K., Sreekumar K; Chem.Comm; 2011, 47, 12910-2912

[24]   E. Proietti, F, Jaouen, M. Lefevre, N. Nat commun, 2011, 2, 416

[25]   M. Lefevre, E, Proietti, F. Jaouen and J.P dodelet, Science 2009, 324, 71-74

[26]   G. Wu, K. L More, C.M Johnston and P. Zelenay, Science, 2011, 332, 443-447

[27]   Cristina G, Markus A, Nano Today (2011) 6, 366-380.

[28]   P. Halili, H. Changting, C. Jinhua, L. Bo, K. Yafei, Z. Xiaohua, J Solid State Electrochem, 2010, 14:169

[29]   H. C. Liang, F. Chen, R.G. Li, L. Wang, Z. H. Deng, Electrochim. Acta, 2004, 49:3463

[30]   R.V. Parthasarathy, C.R. Martin, Nature 369, 1994, 298–301.

[31]   H. Adam, M. Agata, A. Lewenstam, Talanta 41, 1994, 323–325.

[32]   C. Coutanceau, M.J. Croissant, T. Napporn, C. Lamy, Electrochim. Acta 46, 2000, 579–588.

[33] H. Nguyen Cong, K. El Abbassi, P. Chartier, Electrochem. Solid-State Lett.3 (2000) 192–195.

[34] Z. Ding, C.M. Johnston, and P. Zelenay, ECS Trans. 2010, 33(1): 565-577

[35] G. Wu, K.L. More, C.M. Johnston, P. Zelenay, Science, 322(2011) 443-447

[36] B. Merzougui, A. Hachimi, A. Akinpelu, S. Bukola and M. Shao, Electrochim. Acta, 2013, 107, 126-132.

[37] L. Fu, S-J. You, G-Q. Zhang, F-L. Yang, X-H. Fang, Z. Gong, J. Biosensors and Bioelectronics, 2010, 26(5): 1975-1979

[38] P. Ayala, A. Gruneis, C. Kramberger, M.H. Rummeli, I.G. Solorzano, J.F.L. Freire, T. Pichler, The Journal of Chemical Physics 127 (2007) 184709.

[39] F. Tuinstra, J.L. Koenig, Raman Spectrum of Graphite, The Journal of Chemical Physics 53 (1970) 1126–1130.

[40] M. Lefèvre, E. Proietti, F. Jaouen, J.P. Dodelet, Science, 2009,324, 71- 74.

[41] X. Li, H. Wang, J.T. Robinson, H. Sanchez, G. Diankov and H. Dai, J. Am. Chem. Soc., 2009, 131, 15939-15944.

VITAE

Name: Bukola Saheed Abidemi

Nationality: Nigerian

Date of Birth: 20 April, 1982

E-mail: abidemisaheed20@yahoo.com

Address: Department of Chemistry, Federal University of Technology, Akure.

Academic Background: Federal University of Technology Akure, Ondo-State, Nigeria.

(Bachelor Degree in Chemistry, 2008)